MITIGATING DISTRIBUTION FEEDER VOLTAGE RISE OPTIMALLY USING AN ON-LOAD TAP CHANGING TRANSFORMER AND SMART INVERTERS

D.I. Manamperi

(178623P)

Dissertation submitted in partial fulfillment of the requirements for the Degree Master of Science in Electrical Engineering

Department of Electrical Engineering

University of Moratuwa

Sri Lanka

June 2021

DECLARATION OF THE CANDIDATE AND SUPERVISOR

I declare that this is my own work and this dissertation does not incorporate without acknowledgement any material previously submitted for a Degree or Diploma in any other University or institute of higher learning and to the best of my knowledge and belief it does not contain any material previously published or written by another person except where the acknowledgement is made in the text.

Also, I hereby grant to University of Moratuwa the non-exclusive right to reproduce and distribute my dissertation, in whole or in part in print, electronic or other medium. I retain the right to use this content in whole or part in future works (such as articles or books).

……

Signature: Date: 11-08-2021

(D.I. Manamperi)

The above candidate has carried out research for the Masters Dissertation under our supervision.

…….

Signature of the supervisor: Date 11-08-2021

(Dr. L.N. Widanagama Arachchige)

…….

Signature of the supervisor: Date 11-08-2021

(Prof. J. B. Ekanayake)

ACKNOWLEDGMENTS

I take this opportunity to express my profound gratitude to all those who contributed to completing this research.

My supervisors Prof. J. B. Ekanayake and Dr. L.N. Widanagama Arachchige, have given me the most significant support and guidance throughout the research project. I express my deepest gratitude for their guidance and advice during my work. Also, I am thankful for their valuable contribution in reviewing my writing, making corrections to improve, and finalizing the research papers and the thesis.

I am also thankful for all the lecturers who provided their valuable suggestions in progress review presentations.

Finally, I would like to thank my family members for their support provided during the research work.

ABSTRACT

Higher utilization of distributed generation using solar PV can be observed in recent years due to the gradual reduction of solar panel cost. More additions of solar PV generation in the LV grid can be expected in the future. One of the major challenges encountered by distribution grid operators due to high solar penetration is the voltage rise at the far end of the distribution lines. The centralized control of PV inverters and other controllable devices such as on-load tap changer transformers are a potential solution to solve the voltage rise problem. Optimum centralized control is a heavily investigated topic in the recent past. The optimum control of controllable devices in LV grids can prevent the voltage rise while minimising the energy loss due to resistive loss and generation curtailment. Optimum power flow can be utilized for optimum centralized control.

Optimum power flow is a non-convex problem, and there are different solutions to solve it. A sequential mixed-integer second-order cone program-based methodology is suggested in this thesis. According to simulation results, the suggested method has a faster execution time and higher accuracy than the methods discussed in the literature. Also, the thesis proves that the voltage rise can be successfully mitigated by applying the proposed algorithm.

KEYWORDS: Optimum power flow, power distribution system, distributed generation, second-order cone programming

CONTENTS

LIST OF FIGURES

LIST OF TABLES

LIST OF ABBREVIATIONS AND SYMBOLS

Abbreviation	Description
DG	Distributed Generation
GA	Genetic Algorithm
LDC	Line Drop Compensation
LP	Linear Program
LV	Low Voltage
LVDN	Low Voltage Distribution Networks
MINLP	Mixed Integer Nonlinear Program
MISOCP	Mixed Integer Second Order Cone Programming
MPPT	Maximum Power Point Tracking
MV	Medium Voltage
NLP	Nonlinear Program
OLTC	On Load Tap Changer
OPF	Optimum Power Flow
PSO	Particle Swarm Optimisation
PV	Photovoltaic
QP	Quadratic Program
SCP	Sequential Convex Programing
SDP	Semidefinite Program
SLP	Sequential Linear Programing
SOCP	Second Order Cone Program
SQP	Sequential Quadratic Programming
STATCOM	Static Synchronous Compensator
SVC	Static Var Compensator
SVR	Step Voltage Regulators
TO	Tap Operations

1 INTRODUCTION

1.1 Background and motivation

With the gradual decrease of the cost of solar PV (photovoltaic) panels and power conversion equipment, higher PV penetration in distribution networks can be observed throughout the world [1]. Traditional distribution grids are designed to carry power from the distribution transformer to consumers. However, with high PV penetration, reverse power flow from consumers to the distribution transformer can occur. This effect generates problems related to voltage rise.

Distribution networks are predominately resistive, and the X/R ratio is lower than the transmission networks. Therefore, the voltage variation between two points in a distribution line mainly depends on the active power flow, and it increases with the length of the line [2].

Since the direction of power flow changes within a day, distribution network operators need to control the voltage in distribution grids actively. Many control methodologies have been proposed in the literature to solve the voltage rise problems. These control methodologies involve control devices such as on-load tap changers (OLTC), step voltage regulator (SVR), active and reactive power of PV inverters, and energy storage units. Optimum power flow can be used to control the above mentioned devices optimally.

When considering the optimum power flow (OPF) for unbalanced distribution systems, limitations in accuracy, computation time, or optimality can be observed. The optimum power flow technique is introduced in this thesis for overcoming the limitations in optimum power flow of unbalanced distribution systems. In this study, proposed technique is used in a slow time scale to determine tap positions. It is used in a fast time scale to control PV inverters. The performance of the suggested methodology is evaluated by applying it to an IEEE benchmark test case.

1.2 Objectives

The main objective of this research is to develop an optimisation method to prevent voltage rise in low voltage distribution networks (LVDN) with high solar penetration by optimally controlling OLTC and smart inverters.

The specific objective is,

- To develop the optimisation model to be accurate and fast enough for real-time operation with real-time measurements from smart meters

1.3 Scope

Research is focused on the prevention of voltage rise with minimum cost using OLTC and smart inverters. Optimum power flow is used as the control technique for preventing voltage rise. Optimum power flow solving algorithm is developed to overcome limitations in existing methods.

The proposed algorithm is tested for two test cases.

The proposed algorithm is designed to execute in a reasonable time rather than achieving the global optimum.

Short duration voltage fluctuations that occur due to cloud movement is not considered in the proposed optimisation method.

The proposed algorithm is designed for radial distribution networks.

1.4 Overview of the Thesis

Chapter 2 - summarizes the recent research literature, identifies the gaps, and proposes research questions.

Chapter 3 – Formulate the equations, optimisation problem, and solution method

Chapter 4 – Simulation results and analysis

Chapter 5 – Conclusion

2 LITERATURE REVIEW

In this chapter, previous research related to voltage rise prevention using smart inverters and OLTC transformers are discussed. First, papers related to smart inverters are discussed. Then OLTC transformer-related research is discussed. Then, different optimisation techniques are discussed. After that papers associated with the OPF based control of smart inverters and OLTC transformers are discussed, and their drawbacks are examined.

2.1 Smart inverters

The simplest local control strategies of PV inverters include fixed reactive power (fixed Q) and fixed power factor control methods (fixed cos φ). Reactive power outputs of inverters or power factors of inverters are kept at a constant value in these methods. The Characteristic curve is shown in Figure 1. In the cos φ(P) method [3], [4], the power factor of the inverter rely upon the active power generation, and the relationship is expressed as a power factor-active power droop. Power factor – active power diagram of cos φ(P) method is shown in Figure 3. The Q(V) method shown in Figure 4 is based on a reactive power-voltage droop [5]-[4]. Reactive power output depends on the local voltage in this method [3]. Adaptive reactive power -voltage droop control method is proposed in [5]. There, the reactive power absorption ability of inverters close to the transformer is increased by changing droop parameters using a fuzzy inference system. These methods perform better than fixed Q and fixed cos φ methods. Since voltage rise happens near PV inverters at the far end of distribution

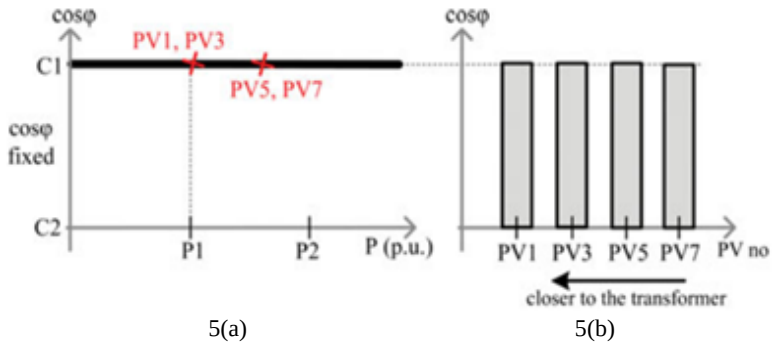

5(a) 5(b)

Figure 1 – Standard reactive power methods. - Fixed cos ϕ. [7].

feeders, the reactive power output of the Q(V) method depends on the location of the PV inverter. The reactive power output of the cos φ(P) method does not have a relation with the PV location.

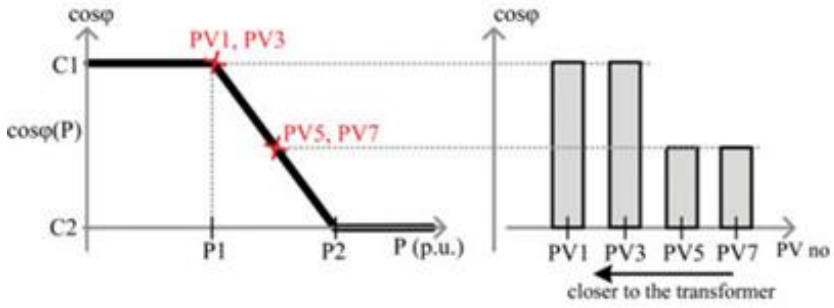

3(a) 3(b)

Figure 3 - Standard reactive power methods - cos ϕ(P) [7]

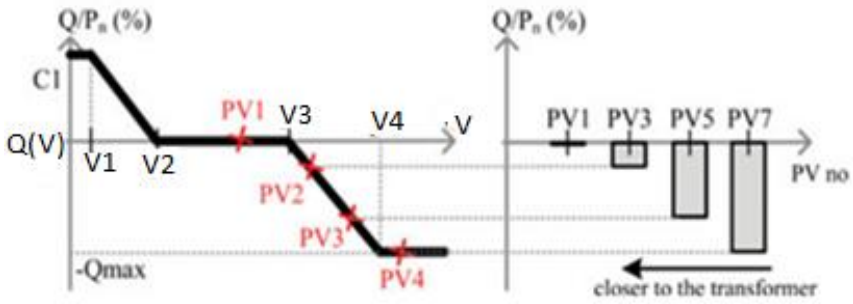

4(a) 4(b)

Figure 4 – Standard reactive power methods - Q(V) [7].

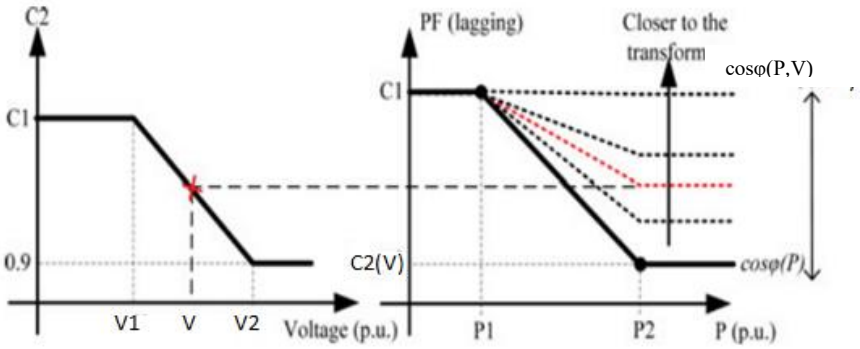

2(a) 2(b)

Figure 2 –. cos φ(P,V) method [7].

An improved cos φ(P, V) method is suggested in [3]. In this method, features of Q(V) are used to assign higher reactive power to inverters further away from the distribution transformer. As shown in Figure 2, the lower power factor C2(V) of the 2(b) graph (cos φ(P)) is selected from the 2(a) graph (Q(V)). There is a higher voltage at end of lines, therefore C2(V) becomes lower when moving away from the distribution transformer. Q(V)/ P(V) method is proposed in [4]. The control methodology is similar to the Q(V) method with the extra active power curtailment feature for the PV inverter when voltage rises at the point of common coupling. The characteristic curve is provided in Figure 5.

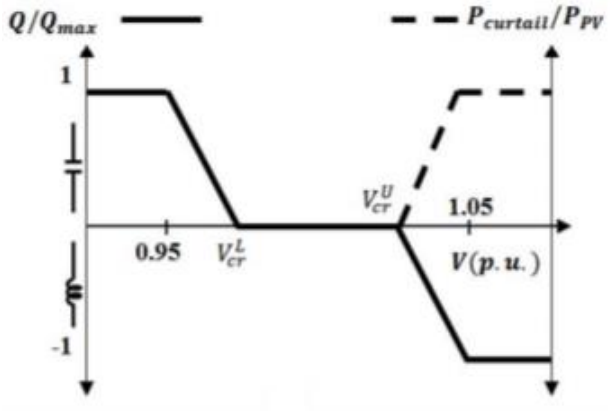

Figure 5 - Q(V)/P(V) method [4]

Uncoordinated reactive power generation or absorption by the inverters can produce further losses. Implementing a communications system is costly. For the effective use of inverters' reactive power capacity with lowest level of communication, a methodology for reactive power management with volt-var control considering inverters' size and sensitivity to the critical bus is presented in [6]. The presented method considers the sensitivity of reactive power of the inverters at distinct locations respective to the critical bus. The furthermost bus with a solar inverter is selected as the critical bus. This method [6] also facilitate other inverters nearby to the critical bus to efficiently use their capacity by supplying reactive power. Inverters are in a queue in descending order of sensitivities. An inverter that has the topmost sensitivity with reactive power availability is set to operate at the lowest power factor.

Although reactive power compensation, works well for inductive lines, the operation in resistive lines is poor [7]. Therefore, the effect of reactive power compensation for low voltage distribution lines is lower compared to active power curtailment. Droop based active power curtailment is discussed in [8]. The control logic used in the simulation is presented in Figure 6. Residences situated downstream on the feeder were needed to curtail more energy than the others (close to the transformer), affecting their revenues according to simulations in [8]. A output power losses (OPL) sharing method among all inverters called active power curtailment with operational power loss sharing (APC-OPLS) method is suggested in [8] to overcome adverse curtailment from downstream inverters. The droop coefficients for APC-OPLS are calculated based on the voltage sensitivity of the system. Active power curtailment of APC-OPLS method is 3% higher than basic APC method according to simulation results of [8].

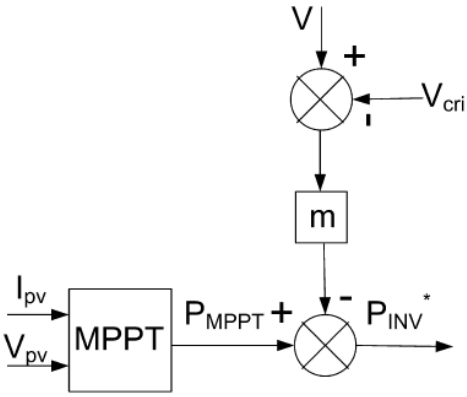

Figure 6 - Droop based active power curtailment of the PV inverter[8]

An approach to droop control of parallel inverters by simulation of a finite-output impedance voltage source and a current source is presented in [7]. Finite-output impedance voltage source and a current source is simulated by controlling the current and voltage output of a single-phase pulse width modulated (PWM) voltage source inverter with a low pass output filter. Benefits in short circuit behavior and voltage harmonic mitigation are reported using the proposed method in [7].

2.2 On load tap changing transformers

The use of OLTC for voltage rise mitigation is widely discussed in the literature. In classical OLTC, an automatic voltage regulator (AVR) is used to keep the measured secondary voltage of the transformer within the reference voltage range. The use of OLTC in a rural European low voltage network to mitigate voltage rise is studied in [9]. The secondary side voltage control of the transformer can cause voltage violations in certain busses, and the investigation of coordinated control between OLTC and PV systems is suggested in [9].

The load drop compensation (LDC) method is a widely used technique to control OLTCs. In the LDC method, the controller of OLTC estimates the voltage drop at the control target point. Then dead-band voltage deviation at the control target point is calculated based on the estimated result, and voltage is controlled through tap operations (TOs) if the voltage at target point exceed the set-point [10].

Static voltage regulators (SVR) are utilized to control the voltage in the middle of distribution lines. The control of SVR can be accomplished using LDC. In conventional methods, OLTC and SVR are operated in the same network through the spatial separation of control zones using LDC impedance [10]. A neural network-based control strategy to control OLTC and SVRs when a static VAR compensator (SVC) is installed in a distribution network is introduced in [10] to mitigate voltage rise.

Three control strategies to control OLTCs are suggested in [11]. These are constant set-point control, time-based control, and remote monitoring-based control. With off-load tap changer, reported PV penetration is 30%, and it was increased to 50% with OLTC using constant set-point control. The remote monitoring-based control has significantly increased the network's PV penetration up to 70%. The time-based control of OLTC has resulted in comparable performance to remote monitoring-based control with more tap operations. OLTC fitted transformer, and network reinforcement is compared from the economic point of view in [12]. According to this study, for smaller PV penetrations (up to 60%), traditional reinforcement is commercially beneficial than the OLTC-fitted transformer.

Coordinated control of distributed energy storage system (batteries) with OLTC transformers for voltage rise mitigation under high PV penetration is suggested in [13].

OLTC operates to keep the voltage within the range of a busbar. The voltage rise is identified if the voltage of any bus is greater than the specified busbar. A charging signal is sent to all batteries when there is a voltage rise. Batteries are discharged at peak load time. Further, tap operation reduction, reducing the utility peak load, and decreasing the line losses during high solar power penetration are achieved using the suggested control scheme.

2.2.1 Drawbacks of OLTC

An growth in tap operations of transformer OLTC due to solar PV generations is reported in [14]. According to [14], the number of tap operations increases on a cloudy day compared to a sunny day. The number of tap operations on cloudy days increases with the PV penetration level. The growth in tap operations in OLTC can reduce the contacts lifespan and stimulate the deterioration of transformer oil during switching process [15]. Therefore, the cost of tap operation also should be included when determining the cost of voltage control in distribution systems.

2.3 Overview of different optimisation methods

A brief overview of the different optimisation methods used to solve the OPF problem is discussed in this section. These optimisation techniques are used in previous researches to solve the OPF problem in transmission and distribution systems. Applications and drawbacks of optimisations techniques discussed in this section are presented in the section 2.4.

2.3.1 Definition of an optimisation problem

An optimisation problem is a problem of finding the best solution from all feasible solutions. It can be represented as follows [16] :

$$minimize\ f(x)$$

$$subject\ to\ g_i(x) \leq 0, \qquad i = 1, \dots., m$$

$$h_j(x) = 0, \qquad j = 1, \dots., p$$

where

- $f: \mathbb{R}^n \rightarrow \mathbb{R}$ is the objective function to be minimised over the n-variable vector x,
- $g_i(x) \leq 0$ are called inequality constraints
- $h_j(x) = 0$ are called equality constraints, and
- $m \geq 0$ and $p \geq 0$.

2.3.2 Evolutionary computation based techniques

Evolutionary computation-based algorithms are inspired by the processes of nature that gradually reach an optimum state. The initial population is generated randomly, and the optimum solution is searched across the feasible set. Genetic algorithms and particle swarm optimisation techniques are extensively utilized for solving OPF problems.

2.3.2.1 Genetic algorithms

A Genetic Algorithm (GA) is a search-based optimisation technique influenced from genetics and natural selection principles. It is utilized to discover optimal or near-optimal solutions to optimisation problems. This algorithm emulates the process of natural selection. The fittest individuals are selected to produce descendants of the next generation. The optimality of the generated solutions is evaluated using the defined fitness function. Best fitted solutions are selected, and a crossover operation is performed to create new solutions to assess fitness. Mutation operation is performed with low probability on some selected solution sets. Converging to a local optimum is avoided from mutation operation.

2.3.2.2 Particle swarm optimisation

Particle swarm optimisation (PSO) is a population-based optimisation approach influenced from movement of bird flocks and schooling fish. The algorithm starts with a population of random solutions, and the search for the optimal solution is achieved by renewing generations.

The potential solutions, called particles, travel in the solution space by following the prevailing optimum particles. Particle swarm optimisation (PSO) is computationally further efficient with regards to both speed and memory usage. Usually, PSO is comparatively less practical and less accurate than GA.

2.3.3 Convex optimisation

Convex optimisation is a mathematical optimisation technique that studies about minimising convex functions over convex sets. Many categories of convex optimisation problems have polynomial-time solution algorithms. Therefore, convex optimisation methods are faster than evolutionary computing-based methods.

2.3.3.1 Convex set

A set C is convex if the line segment between any two points in C lies in C [16].

if for any $x, y \in C$ and any θ with $0 \leq \theta \leq 1$, then

$$\theta x + (1 - \theta)y \in C$$

2.3.3.2 Affine set

A set $C \subseteq R_n$ is *affine* if the infinite line through any two distinct points in C lies in C [16].

if for any $x, y \in C$ and $\theta \in$ R, then

$$\theta x + (1 - \theta)y \in C$$

2.3.3.3 Convex function

A function $f: \mathbb{R}^n \rightarrow \mathbb{R}$ is convex if the domain of f is a convex set and if for all x [16], $y \in$ domain of f, and θ with $0 \leq \theta \leq 1$, then

$$(\theta x + (1 - \theta)y) \leq \theta f(x) + (1 - \theta) f(y)$$

Geometrically, this inequality represents that the straight line between $(x, f(x))$ and $(y, f(y))$, lies above the graph of f as shown Figure 7.

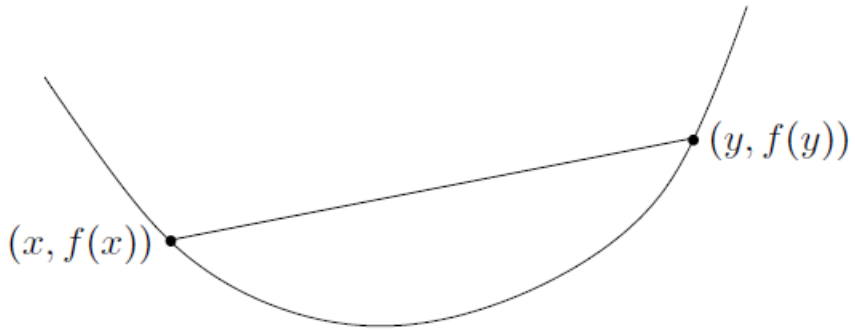

Figure 7 - Graph of a convex function

2.3.3.4 Convex optimisation problem

$$minimize\ f(x)$$

$$subject\ to\ g_i(x) \leq 0, \qquad i = 1, \ldots, m$$

$$h_j(x) = 0, \qquad j = 1, \ldots, p$$

- the objective function $f(x)$ should be convex,
- the inequality constraint functions $g_i(x)$ should be convex,
- the equality constraint functions $h_j(x)$ should be affine

2.3.3.5 Linear program

A linear program is the most straightforward convex optimisation problem. The problem is called a linear program (LP) when the objective and constraint functions are affine. A general linear program has the following form [16].

$$minimize\ c^T x + d$$

$$subject\ to\ Gx\ \leq h$$

$$Ax = b$$

where x ∈ R^n, $G \in R^{m \times n}$, $h \in R^m$ and $A \in R^{p \times n}$.

2.3.3.6 Quadratic program

The convex optimisation problem is identified as a quadratic program (QP) if the objective function is (convex) quadratic and the constraint functions are affine. A quadratic program problem is presented the following form [16].

$$minimize \left(\frac{1}{2}\right) x^T Px + q^T x + r$$

$$subject\ to\ Gx \leq h$$

$$Ax = b$$

where x $\in R^n$ $P \in S^{n+}$, $q \in R^n$, $G \in R^{m \times n}$, $h \in R^m$, $A \in R^{p \times n}$, and ^{T} indicates transpose

2.3.3.7 Second-order cone program

Second-order cone program (SOCP) closely relates to quadratic programming. A SOCP problem is presented the following form [16].

$$minimize\ f^T x$$

$$subject\ to$$

$$\|A_i x + b_i\|_2 \leq c_i^T x + d_i, \qquad i = 1, \ldots, m$$

$$Fx = g$$

where x $\in R^n$ is the optimisation variable, the problem parameters are $A_i \in R^{n_i \times n}$, $b_i \in R^{n_i}$, $c_i \in R^n$, $d_i \in R$, $F \in R^{p \times n}$, g $\in R^p$. $\|x\|_2$ is the Euclidean norm.

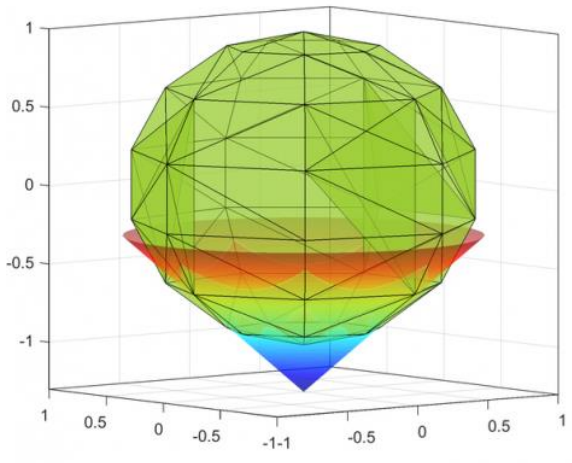

Figure 8 – Feasible region of a SOCP with three variables

As shown in Figure 8, the feasible region of a SOCP problem with three variables is the intersection of the green polyhedron and cone. Green polyhedrons represent the linear inequality and bound constraints. Cone represents the SOC constraint [17].

2.3.3.8 Semidefinite program

In semidefinite programming, linear function subject to the constraints of an affine combination of symmetric matrices is minimised. Some OPF solving methods which use semidefinite programming are presented in the literature review. Semidefinite programming is presented in the below form.

$$minimize\ c^T x$$
$$F(x) \succcurlyeq 0$$

Where $x \in R^n$, $c \in R^n$, $F(x) = F_0 + \sum_{j=1}^{n} x_j F_j$

Here F_0, F_1,…, F_m are symmetric matrices in $R^{m \times m}$ and F(x) $\succcurlyeq$0 means that F(x) is positive semidefinite. Even though this constraint is nonlinear and non-smooth, it is convex. Therefore, semidefinite programs are convex optimisation problems.

2.3.4 Non-convex optimisation problems

Many optimisation problems, including optimum power flow problem, are non-convex optimisation problems. There are two families of methods to solve non-convex optimisation problems. They are local and global optimisation methods. Local optimisations are fast. Finding global optimum is not guaranteed in local optimisation methods. In global optimisation methods, the global optimum is obtained and certified. These are slower than local optimisation methods. The branch and bound method is an example of a global optimisation method.

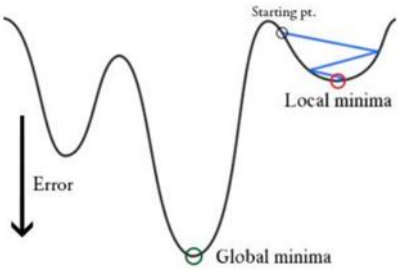

Figure 9 - Global minimum and local minimum

2.3.4.1 Relaxations and approximations

It is possible to make a non-convex optimisation problem convex by introducing modifications to the mathematical model. These modifications can be categorized as relaxations and approximations. As demonstrated in Figure 10, in relaxations, solution space is extended. In approximations, some solution space is neglected. Second-order cone relaxation in the OPF problem is an example of relaxation. Linear approximation from the Taylor series in some OPF formulations is an example of approximations. Generated solution after applying a convex optimisation method for the relaxed problem is guaranteed to be a lower bound to the optimum solution if relaxation is used. This is not true if an approximation is used since some solution space is not considered for optimisation.

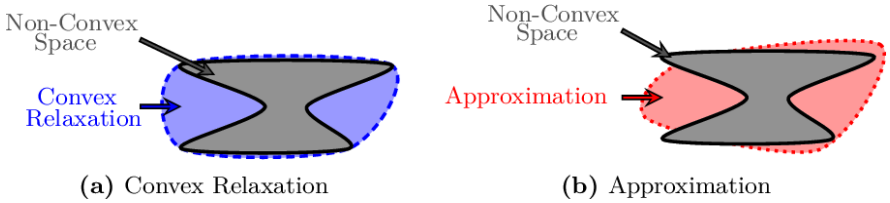

(a) Convex Relaxation (b) Approximation

Figure 10 - relaxations and approximations

2.3.4.2 Sequential convex optimisation

Sequential convex programming (SCP) is a local optimisation technique for non-convex problems, influenced by convex optimisation. The convex portions of the problem are handled efficiently using convex optimisation techniques. The non-convex parts of the problem are modeled by convex functions that are locally accurate [18].

2.3.4.3 Mixed-integer programming

In mixed integer programming, some decision variables are integer values. Execution times of these problems are higher in these problems compared to a similar problem with continuous variables.

Applications of these optimisation techniques, comparison, and drawbacks are discussed in the next section.

2.4 Optimum power flow

Optimum power flow was first proposed by Carpentier in 1962 for offline operation planning of energy networks [19]. Optimum power flow for transmission networks is widely discussed in the previous literature [20], [21], and they are used in day-to-day operations in transmission system control centres [20].

With the increased penetration of renewable energy generation, more randomness and fluctuations occur in power systems. System operators require to update their operation strategies in real-time to react to the fluctuations in renewable generation. The concept of real-time OPF was presented by Bacher and Van Meeteren in 1988 [22]. The real-time OPF (RT-OPF) is designed for responding to the fluctuations of uncertain

parameters in the energy network at every sampling time. These reactions could be either optimal or suboptimal [23]. With the use of learning architecture built using fully connected neuron networks, an RT-OPF approach to achieve a short sampling time considering renewable energy generation was proposed in [24]. The neural networks are trained on different scenarios of the unpredictability in the network.

All the research studies discussed in section 2.1 and 2.2 related to OLTC and smart inverters are based on rule-based centralized or decentralized control schemes. Even though a fast operation is guaranteed, rule-based control schemes are not optimised to achieve their objectives. Optimum power flow can be used as a tool to determine the optimum set points for smart inverters and OLTC in LV networks. With the increase of renewable energy penetration in low voltage distribution networks (LVDN), the use of OPF for controlling power flows in distribution systems is considered. There are several techniques to solve the optimum power flow problem in distribution systems. Even though the primary objective of OPF is not voltage rise prevention in unbalanced distribution networks, some key papers related to unbalanced OPF are discussed here to demonstrate the modifications introduced in this study.

2.4.1 Evolutionary computation techniques for solving OPF problem

Some researchers use evolutionary computation techniques like genetic algorithms (GA) and particle swarm optimisation (PSO) in their centralized control schemes. Grey wolf optimiser is used in [25] to prevent voltage violation in MV distribution systems by minimising curtailing PV power generation and tap movement rate. A genetic algorithm-based method is used in [26] for the centralized cooperation control of sending voltage, and static voltage regulators (SVR), shunt capacitor (SC), and static var compensators (SVC). Evolutionary computation techniques could be time-consuming because of the extensive solution space available with different controllable devices.

2.4.2 Linear programming for solving OPF problem

DC OPF (Direct Current OPF) is widely used in optimisations in transmission networks [20]. It is attained through the linearization of the power flow equations by

assuming all voltage magnitudes to be fixed and all voltage angles to be close to zero. Several linearization approaches are suggested in [21] using piecewise linear approximations to cosine functions and Taylor series approximation to quadratic terms. These methods are designed for transmission networks, and simulations are performed for transmission test cases with low R/X, which are balanced. Due to considered assumptions, results generated from DC OPF are not accurate enough for solving OPF in distribution networks [27], [28].

2.4.3 Semidefinite programming for solving OPF problem

A semidefinite programming (SDP) relaxation of the OPF problem for transmission systems is proposed in [29] based on a rectangular version of power flow equations. The methodology is tested for 300 bus system, and it is reported about the difficulty in solving for extremely large networks. SDP model to minimise power loss and generation cost in unbalanced distribution systems is suggested in [30], based on the bus injection model (BIM). SDP models to minimise generation cost is proposed in [31], based on the bus injection model (BIM) and branch flow model (BFM). BFM is reported to be numerically stable than BIM. The suggested algorithm is tested for IEEE 123 bus distribution system test case and several other test cases without PV generation in [31].

2.4.4 Second-order cone programming for solving OPF problem

Second-order cone programming (SOCP) is widely used to solve the balanced three-phase OPF [32], [33], [34], [35], [27]. In [32], SOCP is used for optimum inverter VAR control in balanced three-phase distribution systems. In [33], three SOCP models are suggested for balanced OPF in transmission networks. In each model, approximations are used to make the voltage phase angle-related equation convex. Approximations are used to make the model close to the actual system, with a tradeoff of computing time in each model. In [36], SOCP is used to solve the OPF problem to decide the optimal dispatch of inverter-interfaced deterministic energy storage in an unbalanced distribution feeder with high solar PV penetration. The solution of the

SOCP is used to start a nonlinear program (NLP) to assure a physically feasible solution.

2.4.5 Convex optimisation for solving OPF problem in unbalanced distribution networks

Convex optimisation-based methodologies are used for voltage control in distribution systems. Optimum power flow for an unbalance three-phase distribution network is represented as a convex quadratic program with the objective of voltage deviation minimisation in [37]. The nonlinear terms in load flow equations have been replaced with first-order Taylor approximations. According to the authors, nonlinear losses behave linearly in mild loading conditions. The algorithm is tested for IEEE 123 bus distribution system test case without PV generation. Sequential quadratic programming (SQP) based technique is used in [38] to solve OPF in unbalanced four-wire distribution systems for improving voltage profile while minimising line losses and generation costs. The algorithm is tested for unbalanced distribution systems with phase A 10.7%, phase B 6.5%, phase C 14.7% PV penetration. Voltage rise is not reported before active control with considered penetration.

2.4.6 Convex optimisation-based methods for tap operation minimisation

Convex optimisation approaches have been used in previous literature to control OLTC. The tap position of OLTC is a discrete variable. Discrete variable are treated as continuous in [39], [40]. Discrete variables are directly used in OPF model with mixed integer programming methods in [41], [42], [43], [44]. A centralized optimum tap control method where the primary objective is minimising the maximum deviation of the voltage profile from 1 p.u. on the whole feeder is proposed in [39]. As the secondary objective considered in [39] is to minimise the number of tap operations. The suggested algorithm is tested for PV penetration of 422%. Further, a convex optimisation approach is used, and the linearization approach is used to convert the problem to convex optimisation problem. A methodology to determine the optimum tap position while reducing voltage deviation from the nominal value, reducing active and reactive power demand of substation is suggested in [40]. Problem is formulated as an SDP, and tap positions are assumed as continuous variables, and voltage

allowance is provided to account for this assumption. The algorithm is tested for IEEE 123 bus distribution system test case without PV generation. An Optimum power flow based methodology for voltage control by controlling OLTC transformers and shunt capacitors is proposed in [41]. . There, Tap operation cost minimisation is considered in multi-objective objective function while weighting it with the cost of line loss minimisation and capacitor switching minimisation for balanced distribution systems. In [41], the trust-region sequential quadratic programming method is combined with the branch and bound approach for solving the resulting mixed-integer nonlinear problem In [39], tap operation minimisation is considered in a multi-objective function while weighting it with voltage deviation minimisation in a 1:100 ratio.

Mixed-integer second-order cone programming (MISOCP) based approaches are used in previous literature to solve OPF with OLTCs and other discrete variables. In [42], MISOCP is used for solving optimal reactive power flow problems in balanced networks. According to simulation results, MISOCP has performed better than MINLP solvers in terms of solution time and power loss reduction. In [43], MISOCP is used for VAR optimisation with network reconfiguration in active distribution systems. Binary variables are used to represent branch status, tap position of OLTC, and steps of discrete VAR compensators. In [44], MISOCP is used for solving the OPF in balanced MV distribution systems with OLTCs. A sequential bound tightening algorithm is applied to ensure that the relaxations are tight.

2.4.7 PV curtailment minimisation

PV curtailment minimisation and line loss minimisation are used as objectives in several studies. In [31], SDP-based OPF is created using BFM and line loss minimisation as the objective. In [36], line loss minimisation is used as an objective along with voltage deviation minimising and battery degradation minimisation in an NLP OPF model. In [38], line loss minimisation and curtailment minimisation is considered as parts of objective function along with voltage unbalance minimisation and inverter loss minimisation. Objectives are weighted according to customized weights. In [44], line loss minimisation and voltage deviation minimisation is tested as an objective in MISOCP based OPF.

2.4.8 Drawbacks in use of convex optimisation for solving OPF problem

However, Obtaining exact solutions is not possible for some practical three-phase distribution systems due to the assumptions considered in relaxations and approximations [10], [20], [45]. According to [45], when simulated for real world test cases, many instances of OPF return semidefinite relaxations with optimal solutions of high rank, which are not exact. Limits of the SDP approach are highlighted in [46] by providing transmission system test cases that fail to give a physically meaningful solution with a non-zero duality gap. A rank minimisation algorithm is suggested in [45] to improve semidefinite relaxation. In [47], the objective function is modified using a heuristic method to extract rank-1 solutions from low-rank solutions. The above methods represent OPF as an SDP, and the computing time of SDP increases rapidly with the number of variables compared to the second-order cone programming (SOCP) approach [33], [27] [48], [49]. Also, SDP solvers are still not numerically robust [36].

SOCP relaxation also provides infeasible solutions to OPF in some conditions [28], [50]. In [50], proofs are provided for balanced SOCP OPF relaxation, to be exact, under some conditions. However, these conditions cannot be satisfied in many practical networks. Increasingly tightening cutting planes are used in [35] and [27] to extract physically meaningful solutions to balanced OPF after applying SOC relaxation. The current value generated from SOCP is used as the upper bound for the current value in the next iteration. According to simulation results, an exact solution is obtained after thirty iterations of SOCP. In [33], a heuristic method is suggested to extract feasible solutions from relaxed OPF problem. There, one variable with the least cost is fixed from the previously obtained solution of SOCP, and SOCP is executed again. This procedure is performed again and again until the solution is feasible.

2.4.9 Non-convex optimisation approaches for solving OPF problem

2.4.9.1 Sequential convex programming for solving OPF problem

Sequential convex programming is another approach that is used to solve the non-convex optimisation problem. In this approach, the convex part of the problem are optimized exactly. The non-convex part of the problem are modelled by convex functions which are locally accurate [18]. Sequential linear programming (SLP) and Sequential quadratic programming (SQP) can be categorized as sequential convex programming methods.

Sequential linear programming (SLP) methods are suggested in previous literature to solve OPF. In SLP, the original nonlinear program (NLP) is converted to a linear program (LP) using a linear approximation of the objective function and constraints about an initial estimate of the optimal solution. The resulting LP is then solved, a new linearization is done about the new solution point, and the process is performed again and again until convergence [20]. In [51], [52], SLP is utilized for solving the OPF problem in transmission networks. In [51], current-voltage formulation is used. In [52], power flow equations in polar coordinates are used.

Sequential quadratic programming (SQP) methods are utilized in previous literature to solve OPF. In SLP, the original non-linear program (NLP) is reduced to a quadratic program (QP) which approximates the NLP problem about a specified operating point. Next, the QP sub problem is solved to optimality. The optimal solution of the QP sub problem then provides the initiating point for the next SQP iteration, and the process is repeated until convergence [20]. In [41], to solve MINLP resulting from the OPF problem with OLTC and shunt capacitors, the trust-region sequential quadratic programming method is combined with the branch and bound. In [22], SQP with multiple start points is used to solve the OPF problem in an unbalanced distribution system.

2.4.9.2 Global optimisation for solving OPF problem

Global optimisation methods are used to obtain the global optimum solution for OPF. Branch and bound techniques are utilized to solve global optimisation problems. In

[53] branch and bound-based global optimisation method is suggested to solve OPF in unbalanced distribution systems. Despite having the global optimum, branch and bound-based methods are time-consuming [54] since there are more than three iterations of convex optimisation programs to be solved.

2.4.9.3 Local optimisation methods for solving OPF problem

Local optimisation methods are used to obtain a local solution to OPF. In [55], the predictor-corrector interior-point algorithm is used to obtain exact local solutions to OPF for an MV distribution system with voltage rise. There is a tendency of converging to the local optimum close to the start point in local optimisation methods [14]. Compared to that, the utilization of convex relaxations provides the guarantee of providing the global optimum for situations where the duality gap is zero.

In this thesis, a modified version of the rectangular voltage-current formulation of the three-phase branch flow model was used with some approximations and relaxations to make the problem convex (SOCP). Sequential MISOCP methodology is suggested to achieve exact solutions by limiting the solutions space gradually to load flow solutions that are solved, including the previous MISOCP outputs. Currents from load flow with gradually decreasing constants are used as cutting planes for second-order cone relaxations. Sufficiently exact solutions are obtained after three iterations of the optimisation program resulting in lesser computation time. Two-time scale optimisations are suggested to minimise tap operations, curtailment and lines losses while reducing voltage rise. In slow time scale, tap operations changing is considered with curtailment and line loss minimisation. In fast time scale optimisation, curtailment and line loss minimisation is considered. The slow time scale optimisation is performed once in an hour or if infeasible solutions are provided by the fast time scale optimisation. The fast time scale optimisation is performed once in every ten minutes.

3 METHODOLOGY

3.1 Problem formulation

Kron reduction technique was used to reduce the four-wire distribution system to a three-wire system [56]. It was assumed that neutral was grounded at multiple points.

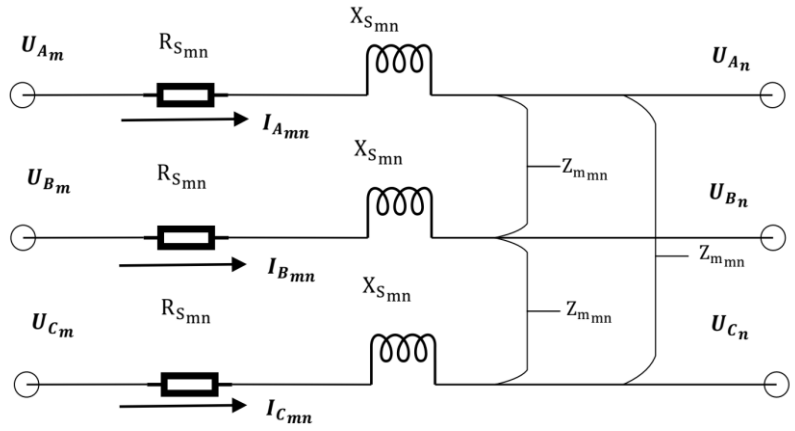

Figure 11 – Diagram of m-n line segment

For the m-n line segment shown in Figure 1, from the power balance of the three-phase lines, the equation (1) was derived [31], [37]. Power flown to node m equals the summation of power flown out of node n, line loss, and power generation/consumption at node n.

$$\begin{bmatrix} \boldsymbol{S_{A_{mn}}} \\ \boldsymbol{S_{B_{mn}}} \\ \boldsymbol{S_{C_{mn}}} \end{bmatrix} = \sum_{k:(j,k)\in E} \begin{bmatrix} \boldsymbol{S_{A_{nk}}} \\ \boldsymbol{S_{B_{nk}}} \\ \boldsymbol{S_{C_{nk}}} \end{bmatrix} + diag\left(\begin{bmatrix} Z_{\mathrm{s_{mn}}} & Z_{\mathrm{m_{mn}}} & Z_{\mathrm{m_{mn}}} \\ Z_{\mathrm{m_{mn}}} & Z_{\mathrm{s_{mn}}} & Z_{\mathrm{m_{mn}}} \\ Z_{\mathrm{m_{mn}}} & Z_{\mathrm{m_{mn}}} & Z_{\mathrm{s_{mn}}} \end{bmatrix} \begin{bmatrix} \boldsymbol{I_{A_{mn}}} \\ \boldsymbol{I_{B_{mn}}} \\ \boldsymbol{I_{C_{mn}}} \end{bmatrix} \begin{bmatrix} \boldsymbol{I_{A_{mn}}} \\ \boldsymbol{I_{B_{mn}}} \\ \boldsymbol{I_{C_{mn}}} \end{bmatrix}^{H} \right) + \begin{bmatrix} \boldsymbol{S_{A_n}} \\ \boldsymbol{S_{B_n}} \\ \boldsymbol{S_{C_n}} \end{bmatrix} \quad (1)$$

where,

$\boldsymbol{s_{A_{mn}}} = p_{A_{mn}} + jq_{A_{mn}}$

$\boldsymbol{S_{A_n}} = \mathrm{P^C_{A_n}} - \mathrm{P^G_{A_n}} + P_A^{Cur}{}_n + \mathrm{j}(\mathrm{Q^C_{A_n}} \pm Q^G_{A_n})$

H denotes the Hermitian transpose.

From the expansion of the first, second and third rows, the power flow equations of phases A, B, and C were obtained. By considering the real parts of the first row to describe the active power flow of phase A, Equation (2) was obtained.

$$p_{A_{mn}} = \sum_{k:(j,k)\in E} p_{A_{nk}} + \mathrm{P}_{\mathrm{A_n}}^{\mathrm{C}} - \mathrm{P}_{\mathrm{A_n}}^{\mathrm{G}} + {P_A^{Cur}}_n + \mathrm{Re}\{\boldsymbol{I_{A_{mn}}}^* \times (\mathrm{R}_{\mathrm{s_{mn}}} \boldsymbol{I_{A_{mn}}} + \mathrm{R}_{\mathrm{m_{mn}}} \boldsymbol{I_{B_{mn}}} + \mathrm{R}_{\mathrm{m_{mn}}} \boldsymbol{I_{C_{mn}}})\} \quad (2)$$

By considering the imaginary parts of the first row to represent the reactive power flow of phase A, Equation (3) was obtained.

$$q_{A_{mn}} = \sum_{k:(j,k)\in E} q_{A_{nk}} + \mathrm{Q}_{\mathrm{A_n}}^{\mathrm{C}} \pm Q_{A_n}^{G} + \mathrm{Im}\{\boldsymbol{I_{A_{mn}}}^* \times (\mathrm{R}_{\mathrm{s_{mn}}} \boldsymbol{I_{A_{mn}}} + \mathrm{R}_{\mathrm{m_{mn}}} \boldsymbol{I_{B_{mn}}} + \mathrm{R}_{\mathrm{m_{mn}}} \boldsymbol{I_{C_{mn}}})\} \quad (3)$$

where,

$\boldsymbol{I_{A_{mn}}}$, $p_{A_{mn}}$, $q_{A_{mn}}$ are the complex current, active power and reactive power flowing from node m to n in phase A.

$\mathrm{P}_{\mathrm{A_n}}^{\mathrm{C}}$ and $\mathrm{Q}_{\mathrm{A_n}}^{\mathrm{C}}$ are the real power consumption and reactive power consumption of phase A of node n.

$\mathrm{P}_{\mathrm{A_n}}^{\mathrm{G}}$, $Q_{A_n}^{G}$ and ${P_A^{Cur}}_n$ are the real power generation and reactive power generation and active power curtailment from the PVs and inverters in phase A of node n.

Two new variables, $W_{A_m} = |\boldsymbol{U_{A_m}}|^2$ and $L_{A_{mn}} = |\boldsymbol{I_{A_{mn}}}|^2$ for every bus and every line were introduced. Then variables in non-convex terms (${U_A^R}_n, {I_A^R}_{mn}, {U_A^{Im}}_n, {I_A^{Im}}_{mn}$) of equations (1) and (2) were replaced by values obtained from load flow. The exact equations used are given in Appendix A as equations A1 and A2.

Equations for apparent power flow at node m to n were derived from Equation (4) [31].

$$\begin{bmatrix} \boldsymbol{S_{A_{mn}}} \\ \boldsymbol{S_{B_{mn}}} \\ \boldsymbol{S_{C_{mn}}} \end{bmatrix} = diag\left(\begin{bmatrix} \boldsymbol{U_{A_m}} \\ \boldsymbol{U_{B_m}} \\ \boldsymbol{U_{C_m}} \end{bmatrix} \begin{bmatrix} \boldsymbol{I_{A_{mn}}} \\ \boldsymbol{I_{B_{mn}}} \\ \boldsymbol{I_{C_{mn}}} \end{bmatrix}^H \right) \quad (4)$$

By expanding the first row,

$$\boldsymbol{S_{A_{mn}}} = \boldsymbol{U_{A_m}} \boldsymbol{I_{A_{mn}}}^* \quad (5)$$

where $\boldsymbol{U_{A_m}}$ and $\boldsymbol{U_{A_n}}$ are the complex voltage at node m and n of phase A and are given by $\boldsymbol{U_{A_m}} = U_{A}^{R}{}_{m} + jU_{A}^{Im}{}_{m}$ and $\boldsymbol{U_{A_n}} = U_{A}^{R}{}_{n} + jU_{A}^{Im}{}_{n}$

Similarly, current flown from m to n of phase A, $\boldsymbol{I_{A_{mn}}} = I_{A}^{R}{}_{m} + jI_{A}^{Im}{}_{m}$

After the multiplication of both sides of (5) by $\boldsymbol{S_{A_{mn}}}^*$,

$$\boldsymbol{S_{A_{mn}}} \times \boldsymbol{S_{A_{mn}}}^* = \boldsymbol{U_{A_m}} \boldsymbol{I_{A_{mn}}}^* \times \boldsymbol{S_{A_{mn}}}^*$$

$$\boldsymbol{S_{A_{mn}}} \times \boldsymbol{S_{A_{mn}}}^* = \boldsymbol{U_{A_m}} \boldsymbol{I_{A_{mn}}}^* \times \boldsymbol{U_{A_m}}^* \boldsymbol{I_{A_{mn}}}$$

$$(p_{A_{mn}} + jq_{A_{mn}}) \times (p_{A_{mn}} + jq_{A_{mn}})^* = \boldsymbol{U_{A_m}} \boldsymbol{U_{A_m}}^* \times \boldsymbol{I_{A_{mn}}}^* \boldsymbol{I_{A_{mn}}}$$

After simplifying the above equation, equation (6) was obtained.

$$p_{A_{mn}}^2 + q_{A_{mn}}^2 = \left|\boldsymbol{U_{A_m}}\right|^2 \left|\boldsymbol{I_{A_{mn}}}\right|^2 \quad (6)$$

Then with substitutions, equation (6) was rewritten as:

$$W_{\boldsymbol{A_{mn}}} L_{\boldsymbol{A_m}} = p_{A_{mn}}^2 + q_{A_{mn}}^2 \quad (7)$$

Using Ohm's law, the equation for the relationship between phase A voltage magnitudes was expressed as in (8).

$$\boldsymbol{U_{A_m}} = \left(\boldsymbol{U_{A_n}} - \boldsymbol{I_{A_{mn}}} \mathrm{Z_S} - \boldsymbol{I_{B_{mn}}} \mathrm{Z_m} - \boldsymbol{I_{C_{mn}}} \mathrm{Z_m}\right) \quad (8)$$

To keep the variables in the optimisation program independent of angle and to make equations linear, the square of equation (8) was used for optimisation after some substitutions. Variables in non-convex terms ($U_{A}^{R}{}_{n}, I_{A}^{R}{}_{mn}, U_{A}^{Im}{}_{n}, I_{A}^{Im}{}_{mn}$) of square equation (8) were replaced by values obtained from load flow. The exact equation used is given in Appendix A as equation (A4). Derivation of equation (A4) is provided in Appendix A.

3.1.1 Constraints

3.1.1.1 Voltage constraints

The phase voltage was maintained within ±6% from the nominal value [57]. The following constraint was used to restrict the squared magnitude of voltages within the allowable range.

$$216^2 \leq \left|\boldsymbol{U}_{\boldsymbol{A_m}}\right|^2 \leq 244^2 \quad (9)$$

3.1.1.2 Inverter reactive power constraints

In this research, the inverter maximum active power capacity is assumed as 90% of its apparent power capacity. Therefore, the maximum reactive power absorption or injection is restricted to 43% of the inverter apparent power capacity.

$$-0.43\mathrm{S}_{\mathrm{A_n}}^{\mathrm{G}} \leq Q_{A_n}^{G} \leq 0.43\mathrm{S}_{\mathrm{A_n}}^{\mathrm{G}} \quad (10)$$

3.1.1.3 Inverter active power curtailment constraints

Capability to curtail full active power generation is provided to inverters. However, curtailment of active power is minimised using the objective function.

$$0 \leq P_{A_n}^{Cur} \leq \mathrm{P}_{\mathrm{A_n}}^{\mathrm{G}} \quad (11)$$

3.1.2 Objective function

To minimise the overall cost incurred for maintaining the voltage within the permissible range, the minimisation of the cost of line losses, the cost of tap changing, and the cost of inverter active power curtailment were considered. The cost of 1 kWh is taken as $ 0.11 [14]. The cost per 1 kWh of line losses and curtailment are considered as same.

For slow time scale optimisation, tap operation minimisation is considered. Cost of tap operation minimisation is included in the objective function of the slow time scale optimisation. This optimisation problem is solved once an hour or if fast time scale optimisation is infeasible. In some time instances it is not possible to keep the voltage within bounds with curtailment and reactive power compensation with the tap position set by previous slow time scale optimisation. In those occasions fast time scale optimisation becomes infeasible. In the slow time scale optimisation, loads and generations for one hour ahead are used for determining the average load and average generation values. It is recommended to use load and generation prediction to determine average load and generation when using in real world situations. Since optimisation is performed considering the loads and generations of one hour ahead, 0.11 (cost of 1 kWh) is taken as the weighting factor for line losses and curtailments to weight them against the cost of tap operation reduction in the multi-objective objective function.

For the fast time scale optimisation, only curtailment and line loss reduction is used. Since both components have the same cost, the same weighting factor is used for both.

3.1.2.1 Cost of line losses

Line losses include the cost of Ohmic losses incurred in three-phase cables and neutral. Here, with the available variables, only the losses in three-phase lines for one hour were considered for the objective in slow time scale, as shown in equation (12).

$$Cost\ of\ line\ losses\ =\ 0.11 \times \left\{\sum_{\forall i \in E}(\mathrm{R_{s_i}}) \times \left|\boldsymbol{I_{A_i}}\right|^2 + \sum_{\forall i \in E}(\mathrm{R_{s_i}}) \times \left|\boldsymbol{I_{B_i}}\right|^2 + \sum_{\forall i \in E}(\mathrm{R_{s_i}}) \times \left|\boldsymbol{I_{C_i}}\right|^2\right\} \quad (12)$$

3.1.2.2 Cost of power curtailment

This term includes the cost of power curtailment of every single-phase inverter, and it is expressed as in (13).

$$Cost\ of\ curtailment\ =\ 0.11 \times \left\{\sum_{\forall i \in N_A} P_A^{Cur}{}_i + \sum_{\forall i \in N_B} P_B^{Cur}{}_i + \sum_{\forall i \in N_C} P_C^{Cur}{}_i\right\} \quad (13)$$

3.1.2.3 Cost of tap change

The cost of one tap change is determined by dividing the cost of the tap changer by the maximum number of possible tap changes. MR Eco on-load tap changer is selected as the tap changer for this study. The cost of the tap changer is $ 12755. The number of maximum possible tap operations is 500,000. The cost of tap operation is obtained using equation (14).

$$Cost\ of\ tap\ operation = \frac{12755}{500000} \times \sum_{\mathrm{t}=1}^{9} b_{\mathrm{t}} \times |t_{old} - t| \quad (14)$$

where, t is the tap position of the current time instance. t_{old} is the tap position of the previous time instance. Here, t and t_{old} are integers within 1-9 b_1 - b_9 are binary variables, and only one among them is 1 according to transformer tap position. The magnitude of phase voltage in the transformer is expressed as follows.

$$\boldsymbol{U_{A1}} = 218.64b_1 + 221.63b_2 + 224.63b_3 + 227.62b_4 + 230.62b_5 + 233.61b_6 + 236.61b_7 + 239.60b_8 + 242.60b_9 \quad (15)$$

Here, b_t is a variable in the optimisation program, and values of t are fixed within 1-9. When the old tap position is the same as the previous one $|t_{old} - t|$ term is zero when b_t is one. Therefore, the cost of tap operation is zero for the objective function. When the old tap position is different from the previous one $|t_{old} - t|$ term is positive when b_t is one. Therefore, the cost of tap operation is non-zero for the objective function, and it increases with the number of performed tap operations.

3.1.3 Representation as a convex optimisation problem

The non-linear equality constraint of (7) is non-convex, and it is relaxed in equation (16). Relaxed constrain (16) represents a second-order cone. Then upper bound as an additional linear inequality constraint (equation (17)) is used to add linear cuts to SOC relaxation. This upper bound is reduced in each iteration. Squared current magnitude generated from a load flow using previous iteration's data is used as a part of the upper bound.

$$L_{A_{mn}} \geq \frac{p_{A_{mn}}^2}{W_{A_m}} + \frac{q_{A_{mn}}^2}{W_{A_m}} \tag{16}$$

$$L_{A_{mn}} \leq \left| \boldsymbol{I}_{\boldsymbol{A_{mn}\,(Load\,flow)}} \right|^2 + \frac{10000}{10^{iteration}} \tag{17}$$

The term $\frac{10000}{10^{iteration}}$ in (17) is a constant for a particular iteration. It reduces to 100 in the third iteration. This constant was chosen empirically to allow a larger search space at the first iteration. Additional search space from $\boldsymbol{I}_{\boldsymbol{A_{mn}\,(Load\,flow)}}$ was reduced 10 times for subsequent iteration using $\frac{10000}{10^{iteration}}$ term.

To represent a discrete set of transformer voltages, equation (18) was used. b_1-b_9 are binary variables, and only one among them is 1 according to the required voltage. The primary side voltage of the transformer is assumed to be constant at the nominal value.

$$W_{A_1} = 218.64^2 b_1 + 221.63^2 b_2 + 224.63^2 b_3 + 227.62^2 b_4 + 230.62^2 b_5 + 233.61^2 b_6 + 236.61^2 b_7 + 239.60^2 b_8 + 242.60^2 b_9 \tag{18}$$

This equation set was repeated for the other 2 phases.

From equations (12), (13), and (14), the objective function in (19) was derived. Then the slow time scale optimisation problem is represented as below subjected to the constraints given by (9) to (11), (16) to (18), and (A1), (A2), (A4) for all 3 phases.

$$\text{minimise } 0.11 \times \left\{\sum_{\forall i \in E}\left(\mathrm{R_{s_i}}\right) \times L_{A_i} + \sum_{\forall i \in E}\left(\mathrm{R_{s_i}}\right) \times L_{B_i} + \sum_{\forall i \in E}\left(\mathrm{R_{s_i}}\right) \times L_{C_i}\right\} + 0.11 \times \left\{\sum_{\forall i \in N_A} {P_A^{Cur}}_i + \sum_{\forall i \in N_B} {P_B^{Cur}}_i + \sum_{\forall i \in N_C} {P_C^{Cur}}_i\right\} + \frac{12755}{500000} \times \sum_{\mathrm{t}=1}^{9} b_{\mathrm{t}} \times |t_{old} - t| \quad (19)$$

such that (9) to (11), (16) to (18), (A1), (A2), and (A4) for all 3 phases.

This optimisation problem is a mixed-integer second-order cone program (MISOCP).

Then the fast time scale optimisation problem is represented as below subjected to the constraints given by (9) to (11), (16) to (18), and (A1), (A2), (A4) for all 3 phases.

$$\text{minimise } \left\{\sum_{\forall i \in E}\left(\mathrm{R_{s_i}}\right) \times L_{A_i} + \sum_{\forall i \in E}\left(\mathrm{R_{s_i}}\right) \times L_{B_i} + \sum_{\forall i \in E}\left(\mathrm{R_{s_i}}\right) \times L_{C_i}\right\} + \left\{\sum_{\forall i \in N_A} {P_A^{Cur}}_i + \sum_{\forall i \in N_B} {P_B^{Cur}}_i + \sum_{\forall i \in N_C} {P_C^{Cur}}_i\right\} \quad (19)$$

such that (9) to (11), (16) to (18), (A1), (A2), and (A4) for all 3 phases.

This optimisation problem is a second-order cone program (SOCP).

3.1.4 Solution method

Due to the relaxation in line apparent power equations, solutions generated from the optimisation program do not satisfy the power flow equations in some situations. To mitigate this effect, in this algorithm, the squared line current is upper bounded by a constant as shown in inequality (16). Three or fewer runs of the optimisation program were used while reducing the upper bound of squared current. This acts as an increasingly tightening cutting planes to SOC relaxations in each phase. Because of this upper bound, a sufficiently exact solution can be obtained after the third or fourth iteration of the optimisation program. Here, $\left|I_{A_{mn\,(Load\ flow)}}\right|^2$ is the squared magnitude of the current value generated from the load flow from the previous iteration in OpenDSS. Non-convex terms in unbalance three-phase Dist-flow equations are another obstacle faced when applying convex optimisation. This difficulty was

addressed by keeping non-convex terms as constants in the optimisation program and updating variables in the non-convex terms by running a load flow using OpenDSS. Therefore, optimisation is performed for much larger convex terms with variables ($W_{A_m}, L_{A_{mn}}$, $p_{A_{mn}}, q_{A_{mn}}, Q^G_{A_n}, {P_A^{Cur}}_n$) while variables in non-convex terms (${U_A^R}_n, {I_A^R}_{mn}, {U_A^{Im}}_n, {I_A^{Im}}_{mn}$) acting as constants for the considered iteration of the optimisation program. When the number of iterations increase, updating terms become closer to the solution generated by the optimisation program. This was verified after observing the load flow generated, and the optimisation program generated current magnitudes and voltage magnitudes plots for each iteration. The flow chart of the proposed algorithm is illustrated in Figure 12. This solution approach closely relates to sequential convex programming [18]. Since the optimisation problem is a MISOCP. The proposed solution approach can be categorized as sequential mixed-integer second-order cone programming.

This algorithm was implemented in Matlab with CVX optimisation toolbox [58] and MOSEK as the solver. OpenDSS was used to run the load flow and update variables in non-convex terms.

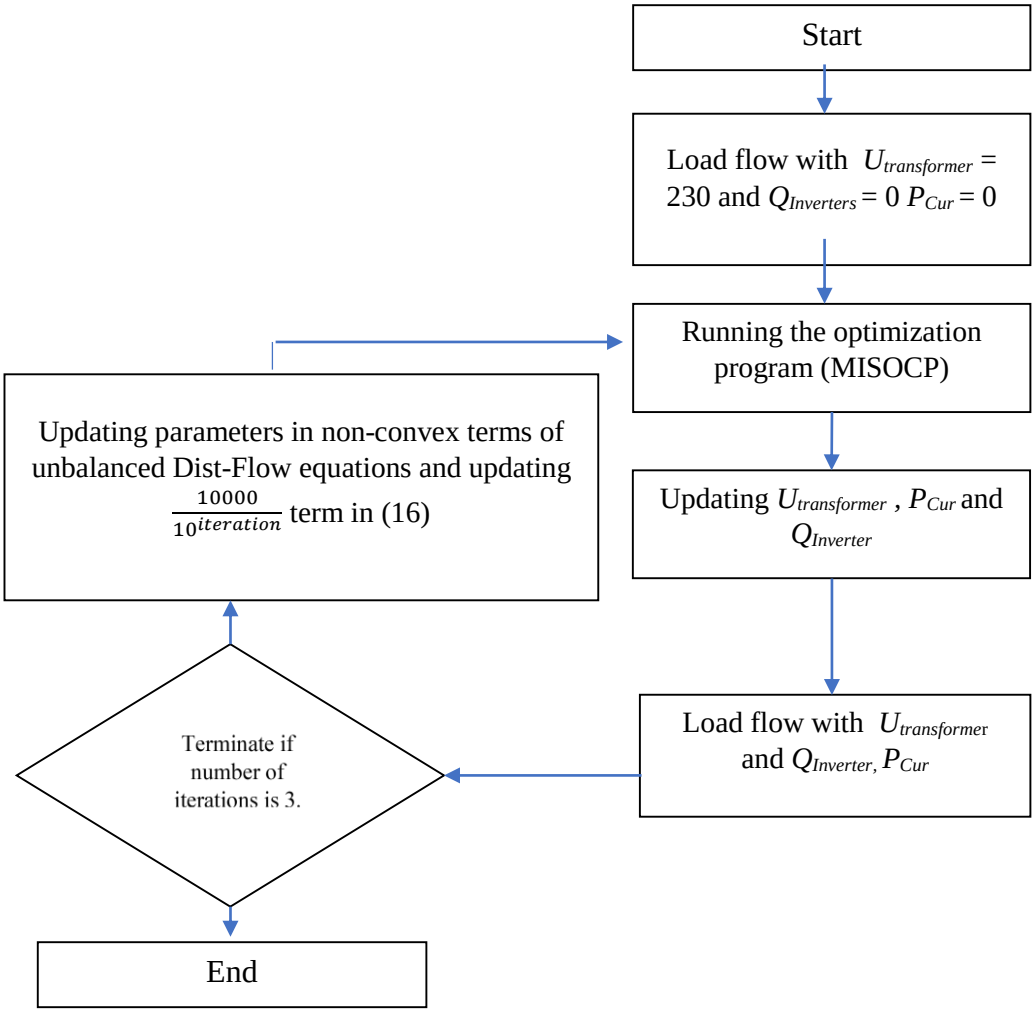

Figure 12 - Flow chart of the OPF solving algorithm for slow time scale optimisation

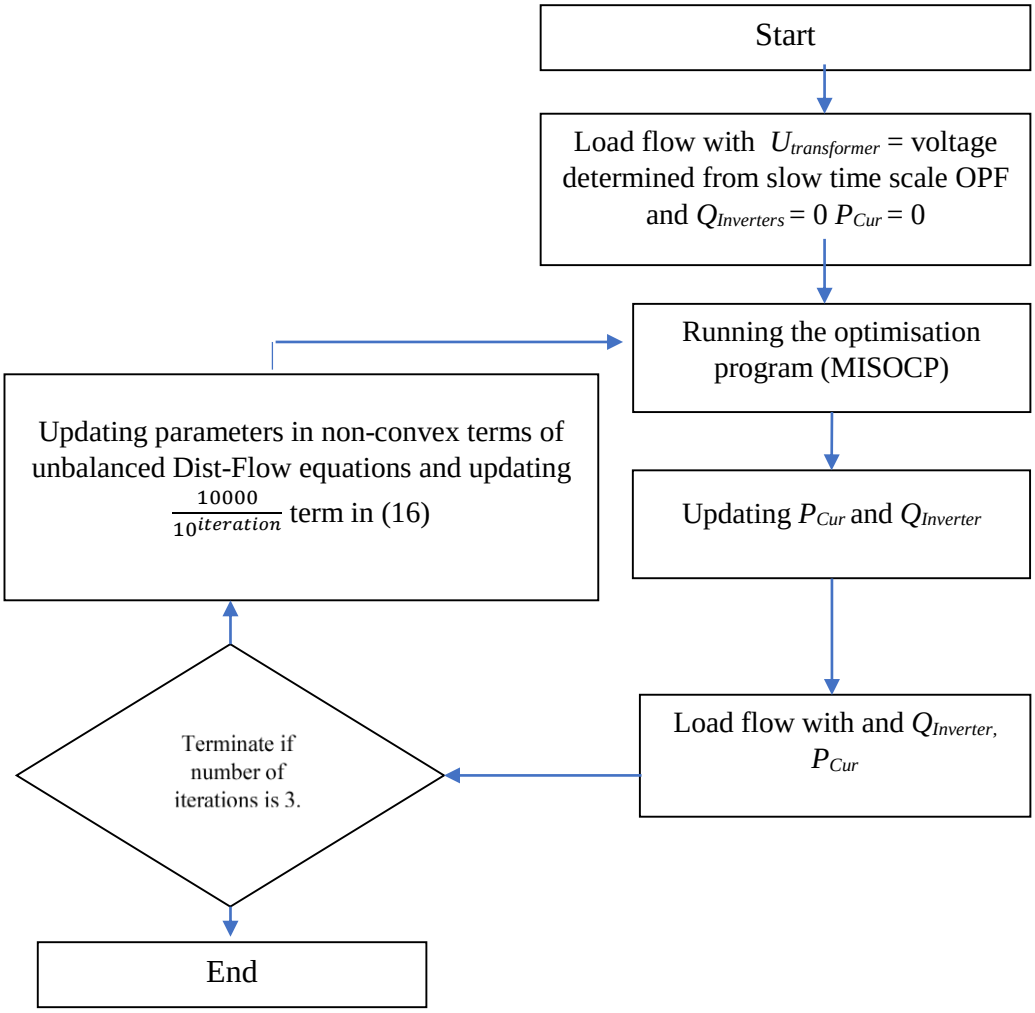

Figure 13 - Flow chart of the OPF solving algorithm for fast time scale optimisation

4 CASE STUDIES

In this section, the simulation results of the suggested method for two distribution systems are analysed. The primary voltage of the transformer was assumed as the nominal (11 kV). The L-N voltages at the transformer busbar are adjusted in ±1.25% voltage steps analogous to the tap positions from 1 to 16 [59].

Details of the transformer are as follows:

Primary voltage (L-L)	11 kV
Secondary voltage (L-L)	416 V
Capacity	0.8 MVA
Vector group	Δ/Y
Reactance (%)	4
Resistance (%)	0.4

For modelling the transformer, the reactance and resistance of the distribution transformer were added to the positive sequence reactance and resistance values of the first line section from bus 1 to 2, as shown in Figure 3. An ideal voltage source was connected to bus 1. The same transformer was used for two case studies. Details of the cables provided by IEEE power and energy society [60] were used for the simulation of two test cases. Simulations were performed in a PC with an Intel Core i7 @ 1.8 GHz processor and 8 GB RAM.

4.1 Test case 1

Test case 1 is a synthesized network with 18 nodes, as shown in Figure 14. This test case was used to demonstrate the voltage control and reactive and active power control throughout the daytime. Nine single-phase consumers are connected to this network. The details of the network are given in Table 1 and Table 7. Cable lengths were extended to obtain a voltage rise with realistic PV generation. This test case is provided

to closely observe the output of the suggested control algorithm for load and generation conditions.

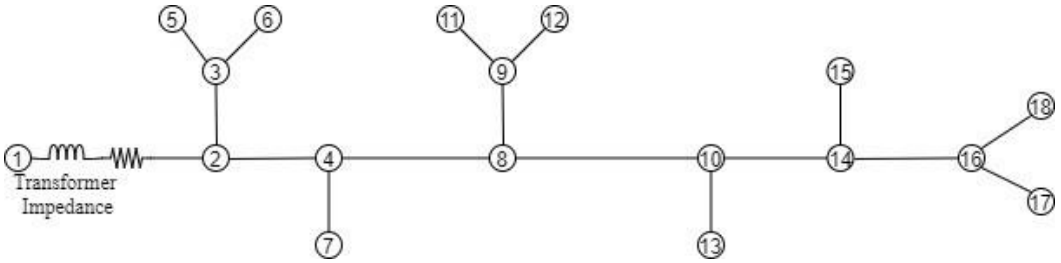

Figure 14 - Network diagram of test case 1

Randomly selected single-phase inverter capacities from 1 kVA to 4 kVA were placed in randomly selected five consumers from available nine single-phase consumers. PV generation profile (Figure 17) that results in a voltage rise was selected for the case study.

Details of the inverter capacities and loads are provided in the Table 1.

Table 1 - Details of loads and inverter capacities of test case 1

Name	**Bus**	**phases**	**Inverter capacity(kVA)**
Load 1	5	B	1
Load 2	6	B	2
Load 3	7	A	0
Load 4	11	A	0
Load 5	12	A	0
Load 6	13	B	4
Load 7	15	B	4
Load 8	17	C	0
Load 9	18	A	4

The details of the cables in each segment are provided in Appendix A. All the cables are underground cables.

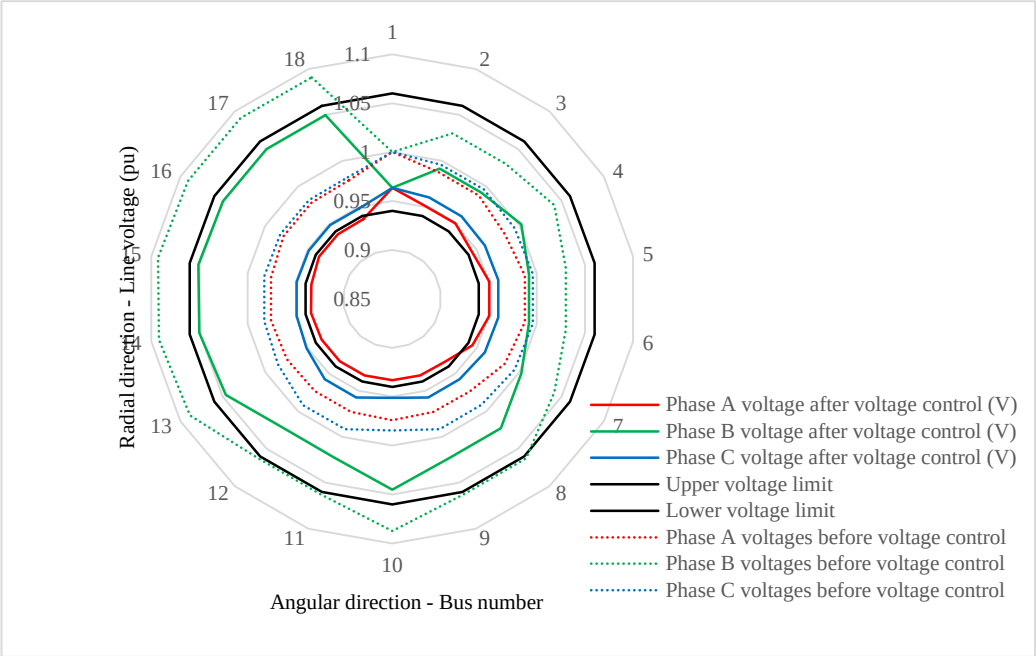

Figure 15 - Voltage profile comparison of case study 1

Voltage rise generated from reverse power flow at 12.00 p.m. is observed in Figure 15. The permissible voltage range is within two black circles. The resulting voltage profile after using the suggested control methodology is also included in Figure 15. The performance of the algorithm from 12.00 p.m. to 12.50 p.m. is considered next.

The voltage profile from 12.00 p.m. to 1.00 p.m. is presented in Figure 16. Voltage values are obtained from load flows simulated using OpenDSS. From Figure 16, voltage rise above 244 V can be seen at the far end of phase B. Active power generation in phase B is comparatively larger as shown in Figure 17. Larger active power generation at node 13 and 15 is the main reason for the voltage rise in phase B. A voltage rise within the allowable range in phase A also can be observed from 12.40 p.m. to 1.00 p.m. when active and reactive power consumption in phase A is close to zero.

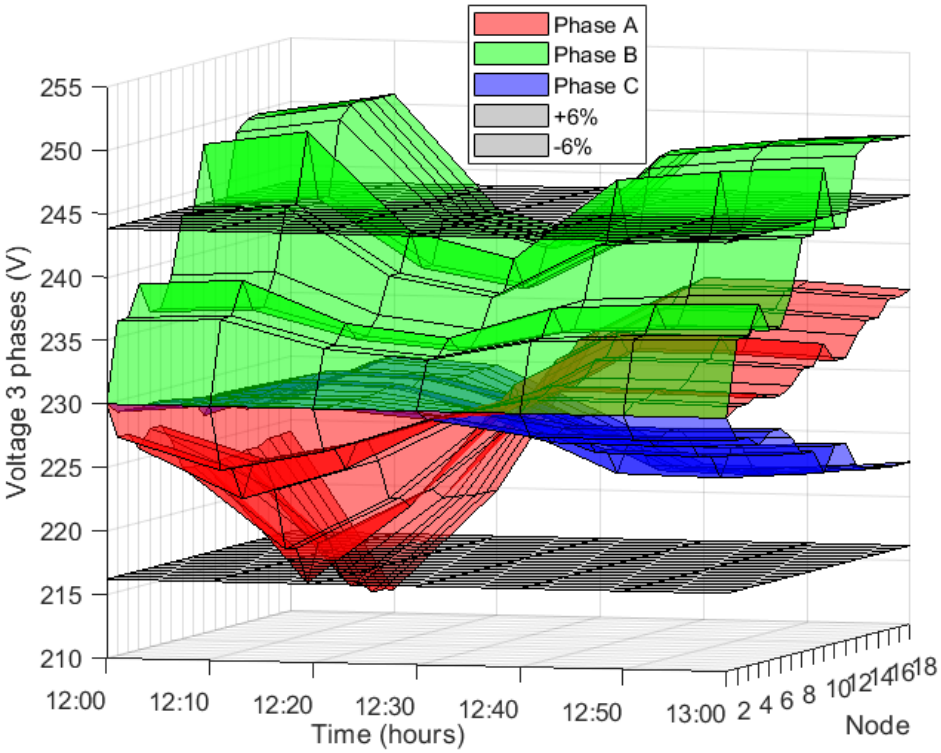

Figure 16 - Voltage profile before voltage control

A low voltage below the permissible range in the far end of phase A can be observed in Figure 16 at 12.10 p.m. and 12.20 p.m. Higher active and reactive power consumption in the far end of phase A has resulted in the low voltage situation. From Figure 18 and Figure 19, higher active and reactive power consumption can be observed. The voltage rise of phase B is reduced to the allowable range at 12.20 p.m. and 12.30 p.m due to active power consumption. Active power consumption in node 15 of phase B can be observed at 12.20 p.m. and 12.30 p.m. in Figure 18 and Figure 19.

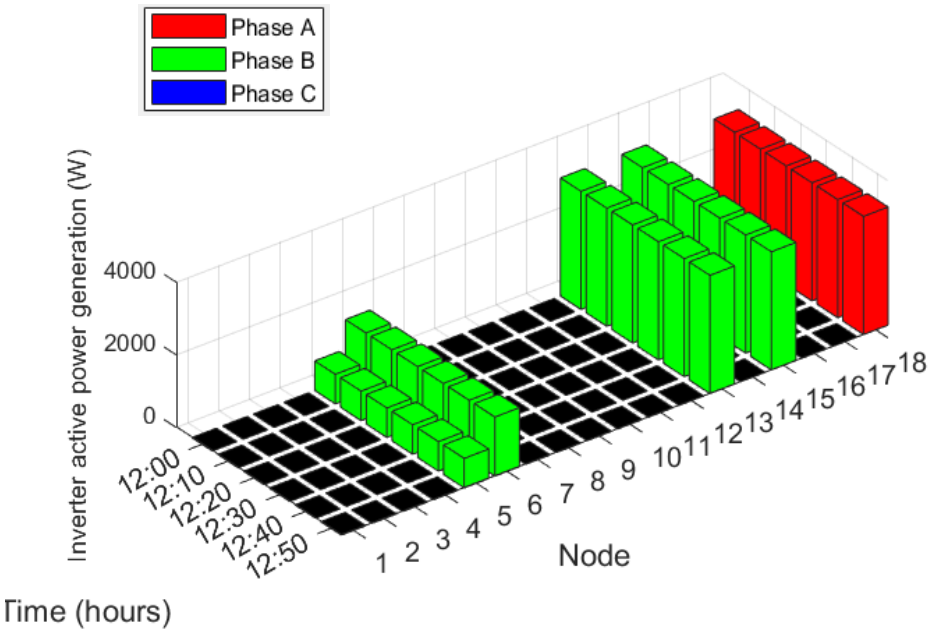

Figure 17 - Active power generation from solar inverters

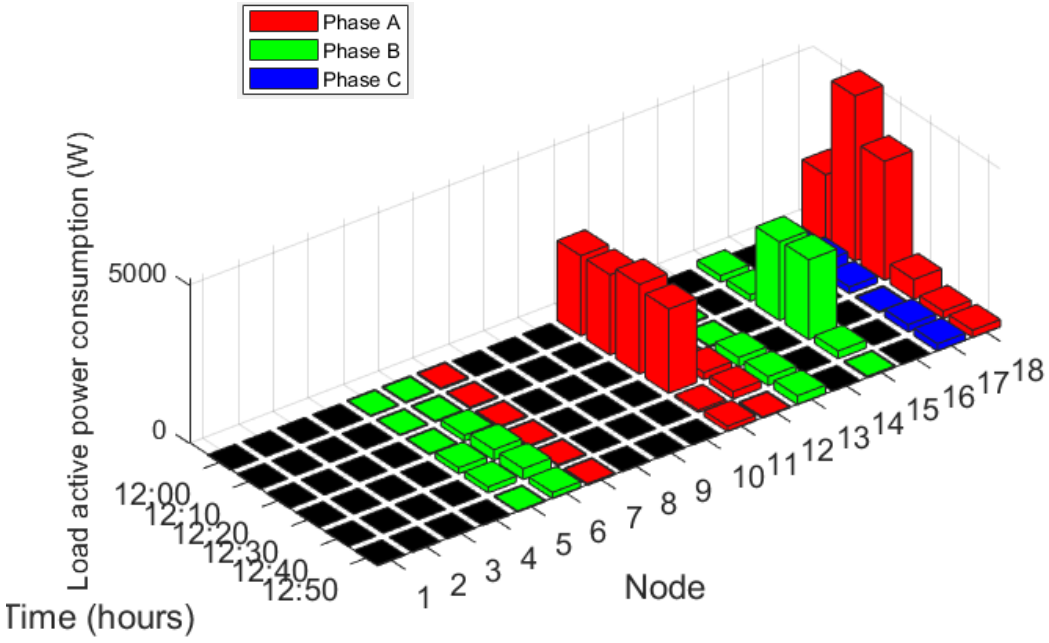

Figure 18 -Active power consumption of loads

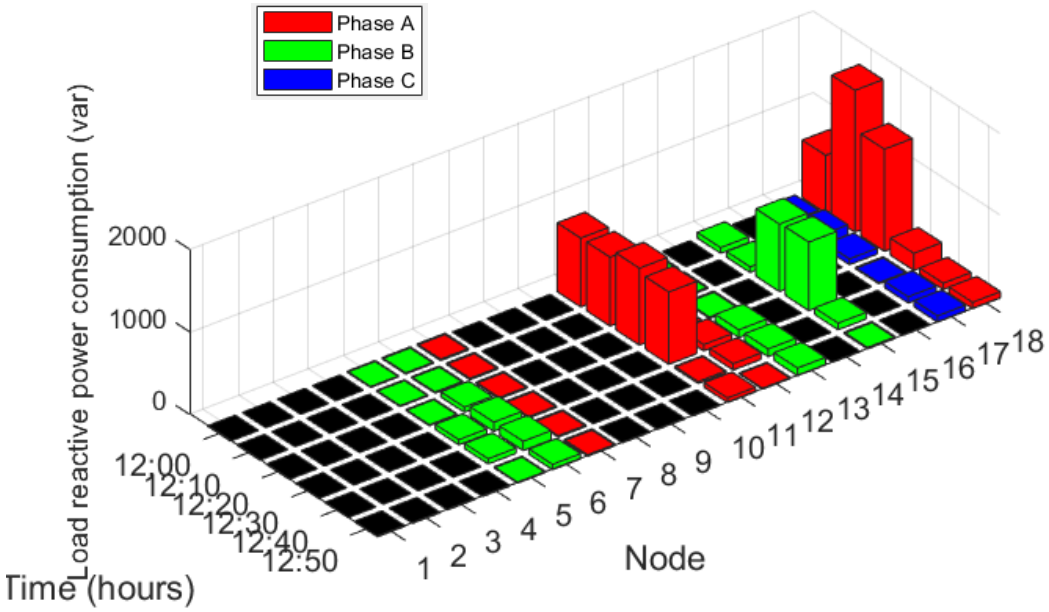

Figure 19 - Reactive power consumption of loads

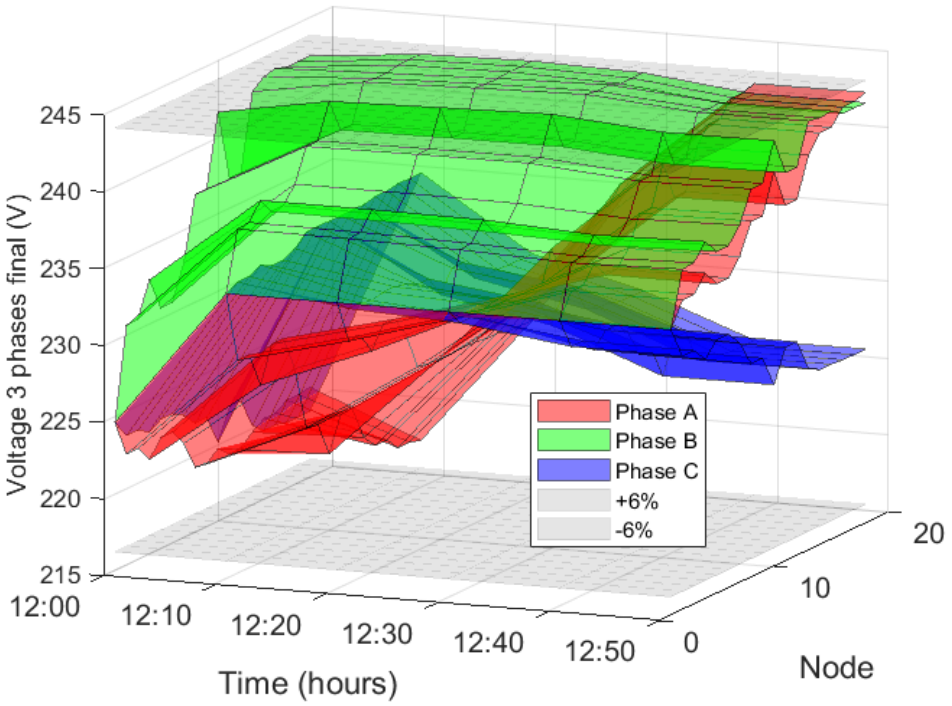

Figure 20 - Voltage profile after voltage control (12.00 p.m. – 12.50 p.m.)

The voltage profile after executing the proposed algorithm can be observed in Figure 20. Voltages of all nodes are within allowable limits. Also, it can be observed that the voltage at the far end of phase B is always close to 244 V. When the voltage is at the maximum possible values, line loss is minimum since the current flown is minimum. Therefore, it can be observed that the line loss is reduced with the proposed algorithm. Voltage is controlled through controlling OLTC, active power curtailment and reactive power compensation.

Voltage control from OLTC can be observed in Figure 20 from the voltage of node 1. Voltage control of each time step within 12.00 p.m to 12.50 p.m. is analysed next.

Voltage control at 12.00 p.m. :-

The default tap position was given as 5, which is corresponding to 230.62 V. Transformer voltage is reduced to 224.63 V at 12.00 p.m. to reduce the voltage rise.

Active power curtailment can be observed at node 15 as shown in Figure 22. This is performed to reduce the voltage rise at phase B.

Reactive power is absorbed from the inverter at node 15 due to voltage rise as shown in Figure 21.

Voltage control at 12.10 p.m. :-

Then at 12.10 p.m. transformer voltage is increased back to 233.61 V to compensate for the low voltage situation at phase A. Fast time scale optimisations with tap position of 12.00 p.m has become infeasible at this moment. Therfore, new tap position is determined again by executing slow time scale optimisation program.

Active power curtailment of phase B at node 15 and node 13 is increased even though the generation and consumption of phase B are the same as in previous time slots. There is an increase in active power consumption in node 18 of phase A at 12.10 p.m.while the transformer voltage is increased to mitigate the low voltage situation as described in the previous paragraph. To keep the voltage level of phase B within the permissible range at 12.10, the active power of node 15 and node 13 is curtailed by more than that at 12.00 p.m.

Voltage control at 12.20 p.m. :-

Transformer voltage is maintained at 233.61 V at 12.20 p.m since fast time scale optimsation is feasible with previous tap position. Reactive power is injected at node 18 to compensate for load reactive power absorption.

Voltage control at 12.30 p.m. :-

Transformer voltage is maintained at 233.61 V at 12.30 p.m since fast time scale optimsation is feasible with previous tap position. At 12.30 p.m. there is less active power curtailment compared to other time instances due to loads in phase B node 15.

Voltage control at 12.40 p.m at 12.50 p.m. :-

Transformer voltage is maintained at 233.61 V at 12.40 p.m and 12.50 p.m. since fast time scale optimsation is feasible with previous tap position.

Generation and consumption in these two-time instances are nearly similar. Therefore similar control strategy can be observed. At 12.40 p.m at 12.50 p.m., Active power curtailment can be observed at node 15 of phase B. Reactive power absorption can be observed in node 13 and 15 of phase B.

Reactive power injection :-

Reactive power injection from inverters can be observed in Figure 23. Reactive power injection from inverter at node 18 of phase A can be observed due to low voltage conditions at phase during 12.00 p.m. to 12.20 p.m. All the inverters inject reactive power corresponding to the reactive power absorption by loads as shown in Figure 19.

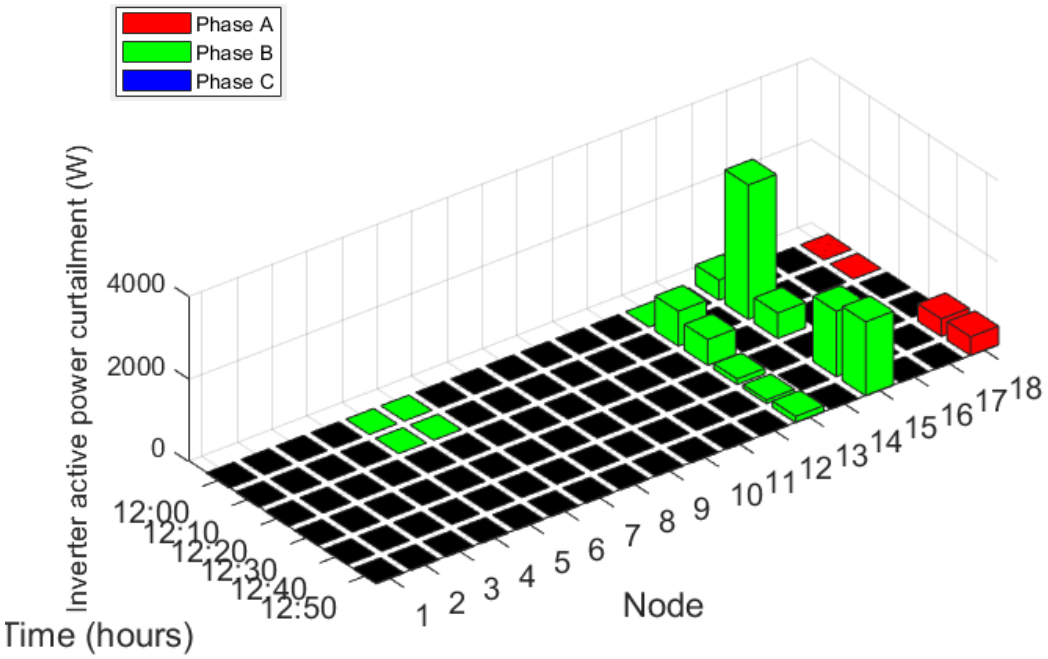

Figure 22 - Active power curtailment from inverters

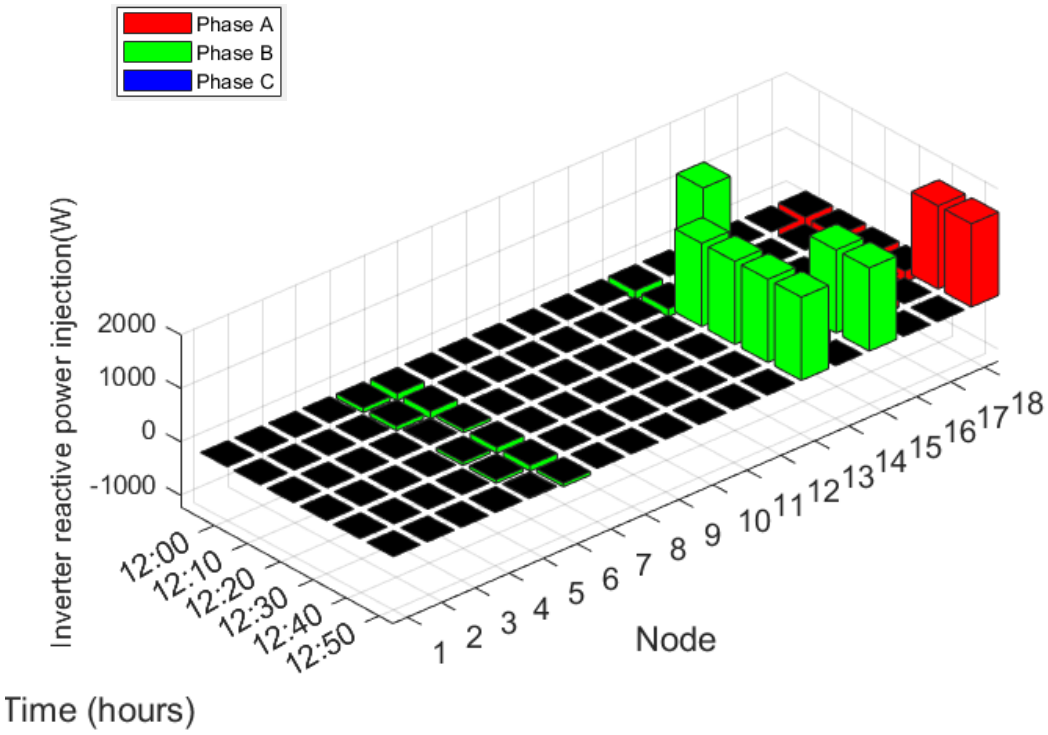

Figure 21 - Reactive power compensation from inverters (absorption)

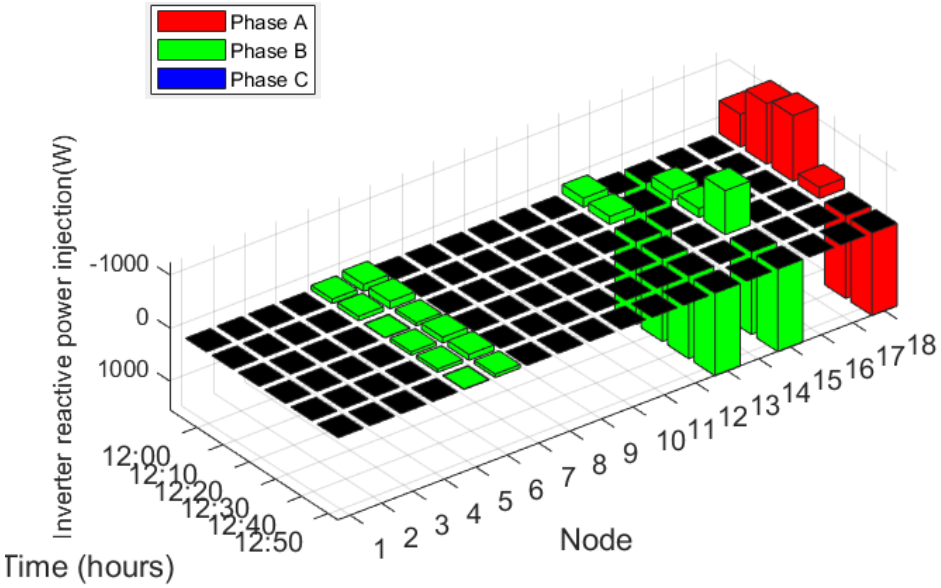

Figure 23 - Reactive power compensation from inverters (injection)

Voltage profile from 10.00 a.m. to 2.50 p.m. is provided in Figure 24. Tap operations are performed in one-hour duration using slow time scale optimisation unless fast time scale optimisation is infeasible. Tap operations performed within one-hour duration are performed due to the infeasibility of fast time scale optimisation using previous tap position. Transformer voltage from 6.00 a.m. to 15.50 p.m. is provided in Figure 25. In most cases, fast time scale optimisation is feasible to solve the OPF during one-hour period between slow time scale optimisations.

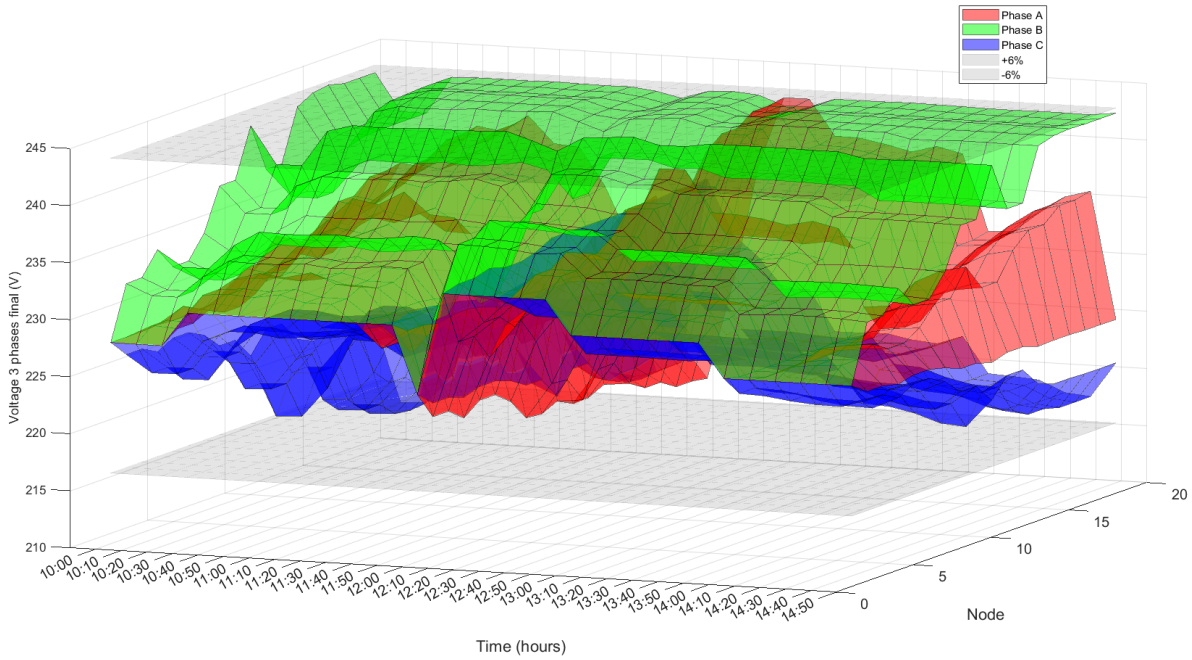

Figure 24 -- Voltage profile after voltage control (10.00 a.m. – 2.50 p.m.)

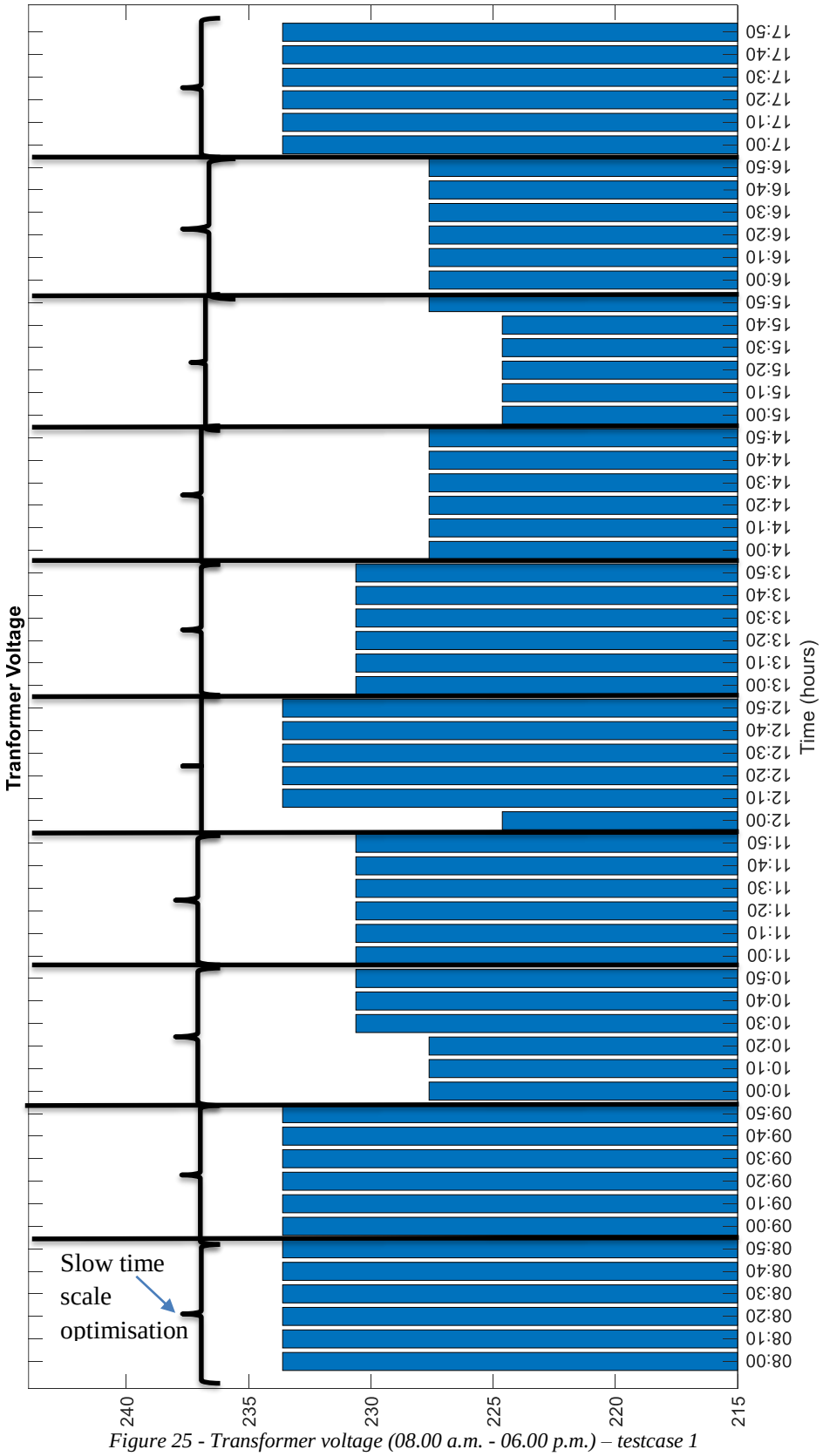

Figure 25 - Transformer voltage (08.00 a.m. - 06.00 p.m.) – testcase 1

Evaluating the exactness of the proposed method is important to investigate the adverse effects of the relaxations and approximations used in the mathematical model. The difference between voltage values obtained from load flow (simulated using OpenDSS) which is simulated using transformer voltage, inverter curtailment, and reactive power compensation values obtained from the optimisation program, and voltage values obtained from optimisations program (simulated using CVX/ Mosek) is analysed next.

$$Voltage\ difference = V_{optimization} - V_{load\ flow} \quad (22)$$

$Voltage\ difference$ is calculated according to equation (22) for all nodes. It is plotted for three iterations of optimisation programs in Figure 26 to Figure 28.

A reduction in differences between two voltage profiles can be observed from the first iteration to the third iteration, as shown in Figure 26 to Figure 28. In Figure 26 , voltage differences above 4 V can be observed. Having this level of voltage difference can generate voltage violations after control since voltage values of the optimisation program are kept within the allowable range. The maximum voltage difference is reduced below 1 V as shown in Figure 28. This is a result of bound tightening in equation (19). From Figure 28, the accuracy of the proposed OPF solving algorithm can be observed. The difference between voltage values obtained from the optimisation algorithm and voltage values obtained from the load-flow executed with curtailment and reactive power values generated from the optimisation program is negligible. This further validated the accuracy of the optimisation method used in this study.

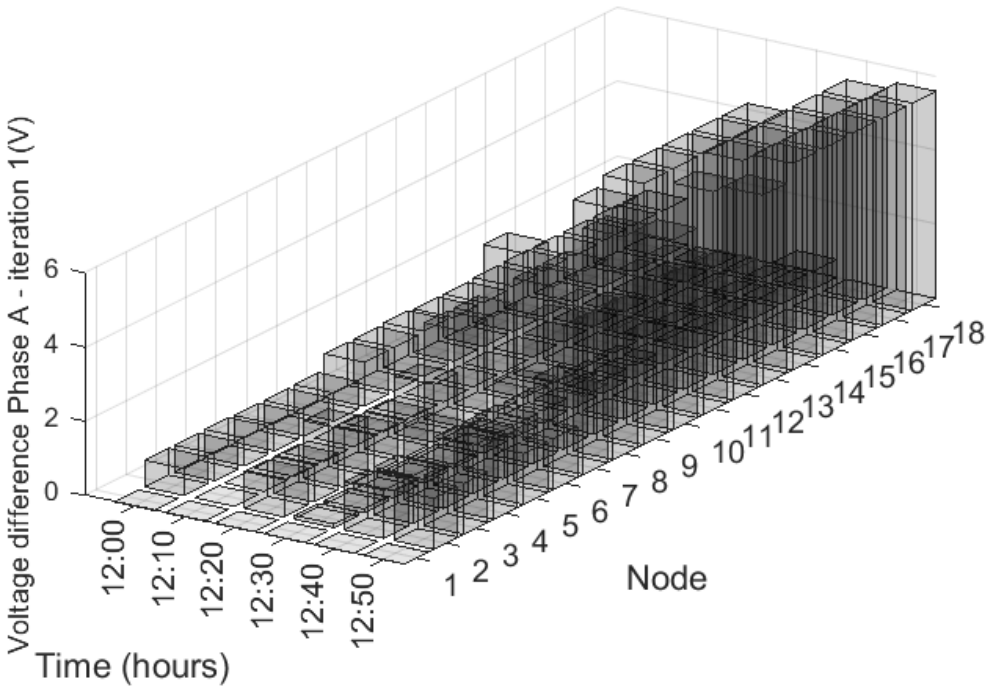

Figure 26 – Voltage difference between load flow and first iteration of optimisation program of phase A

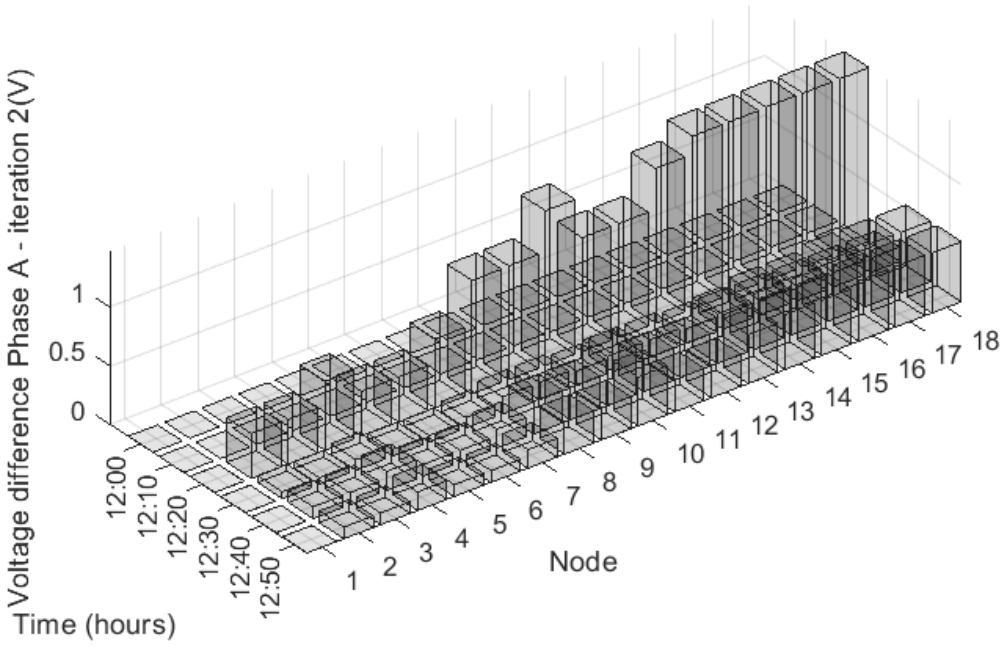

Figure 27 - Voltage difference between load flow and second iteration of optimisation program of phase A

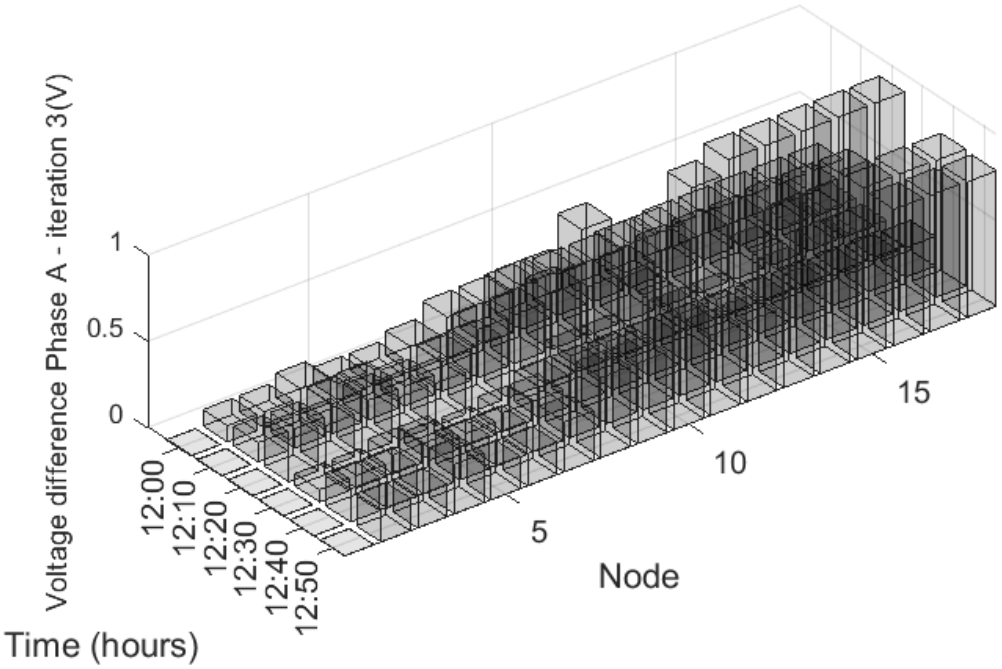

Figure 28 - Voltage difference between load flow and third iteration of optimisation program of phase A

Total line losses of each time instance are compared in the below chart.

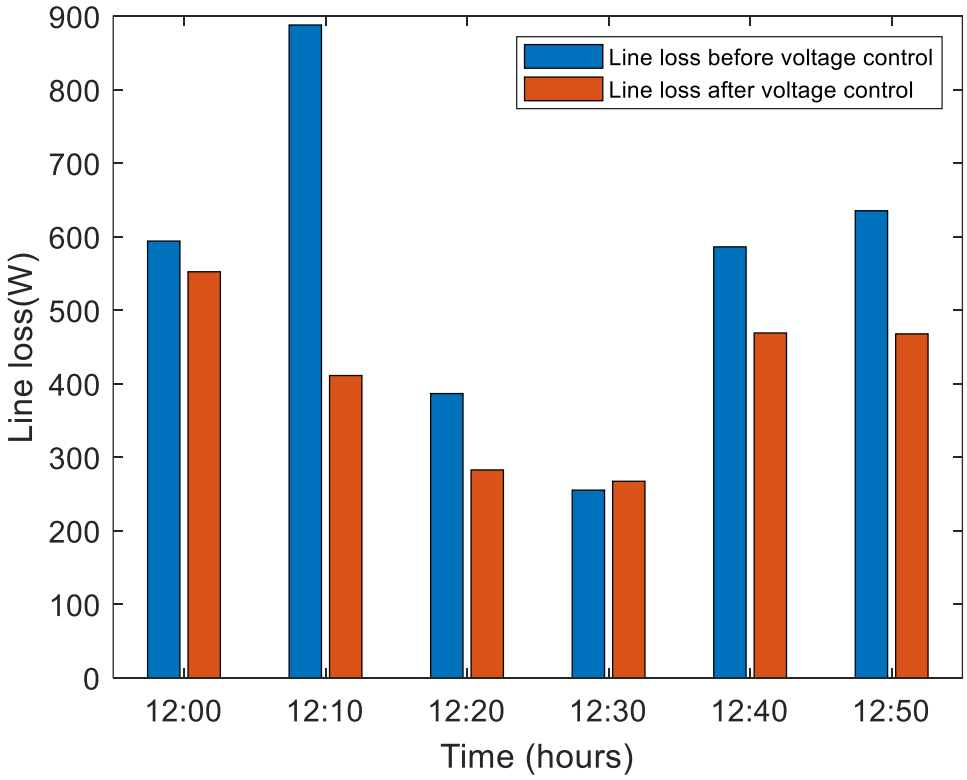

Figure 29 - Line losses in each time instance before voltage control

When analysing Figure 29, line loss reduction can be observed after applying the algorithm. This results from active power curtailment and reactive power control from smart inverters. The algorithm adjusts the reactive power, curtailment, and tap position to minimise the objective function. Line loss is a component in the objective function. Therefore, a reduction in line losses further demonstrates the performance of the algorithm.

4.2 Test case 2

An underground European network provided by IEEE power and energy society was selected as the test case [60]. The network diagram is presented in Figure 30. Nodes with loads at phase A, B, C are marked with red, green, and blue squares, respectively, and load profiles at 12 p.m to 12.50 p.m. are selected. Voltage rise can be observed after 12.10 p.m as shown in Figure 31, Figure 32 and Figure 34.

Randomly selected single-phase inverter capacities from 1 kVA to 7 kVA were placed in randomly selected 45 consumers from available 55 single-phase consumers. Power generation provided in the table depends on the irradiance and efficiency of the inverter.

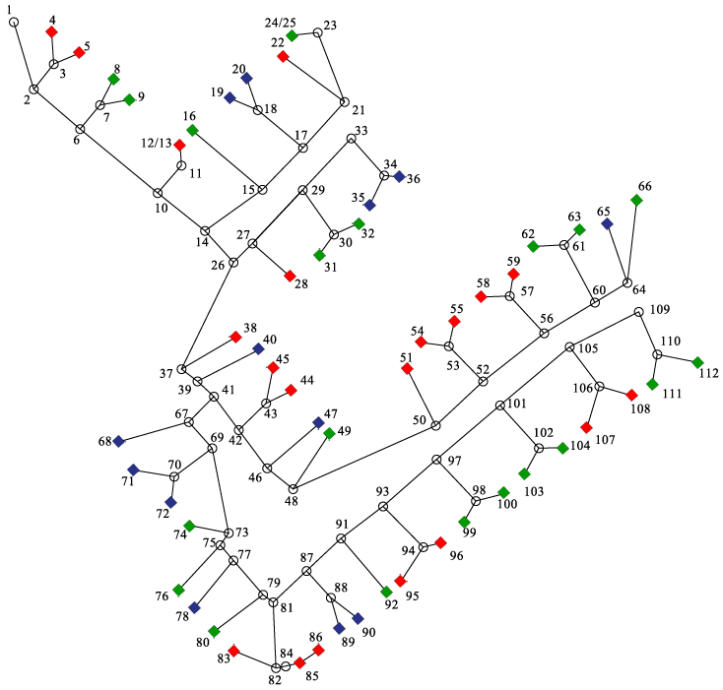

Figure 30 - Network diagram test case 2

PV curtailment compared to PV generation of phase C at 12.10 p.m is presented in Table 2. As shown in the table, reactive power is injected to reduce line losses. Active power curtailments are negligible.

Table 2 - PV generation, curtailment, and reactive power of inverters in phase C (test case 2)

Time	Node	PV generation (W)	PV curtailment (W)	Reactive power generation (Var)
12.10	19	2197.501	2.15E-07	-121.996
12.10	20	732.5003	2.16E-07	-17.1148
12.10	35	2930.001	3.00E-07	-102.625
12.10	36	5127.502	3.34E-07	-15.8734
12.10	40	2197.501	3.42E-07	-751.339
12.10	47	5127.502	3.42E-07	-69.4695
12.10	65	5127.502	8.89E-07	-63.8564
12.10	68	2197.501	3.58E-07	-37.608
12.10	71	2930.001	4.22E-07	-9.3175
12.10	72	1465.001	4.23E-07	-59.8619
12.10	78	5127.502	7.58E-07	-18.9123
12.10	89	5127.502	2729.947	2450.946
12.10	90	4395.002	1729.371	2100.811
12.10	103	5127.502	3027.692	2450.946
12.10	104	5127.502	3364.675	2450.946

Voltage rise generated from reverse power flow at 12.10 p.m. can be observed in Figure 31. The permissible voltage range is within two black circles. The resulting voltage profile after using the suggested control methodology is also included in Figure 31. Only the voltages of some critical nodes are shown in p.u. in Figure 31.

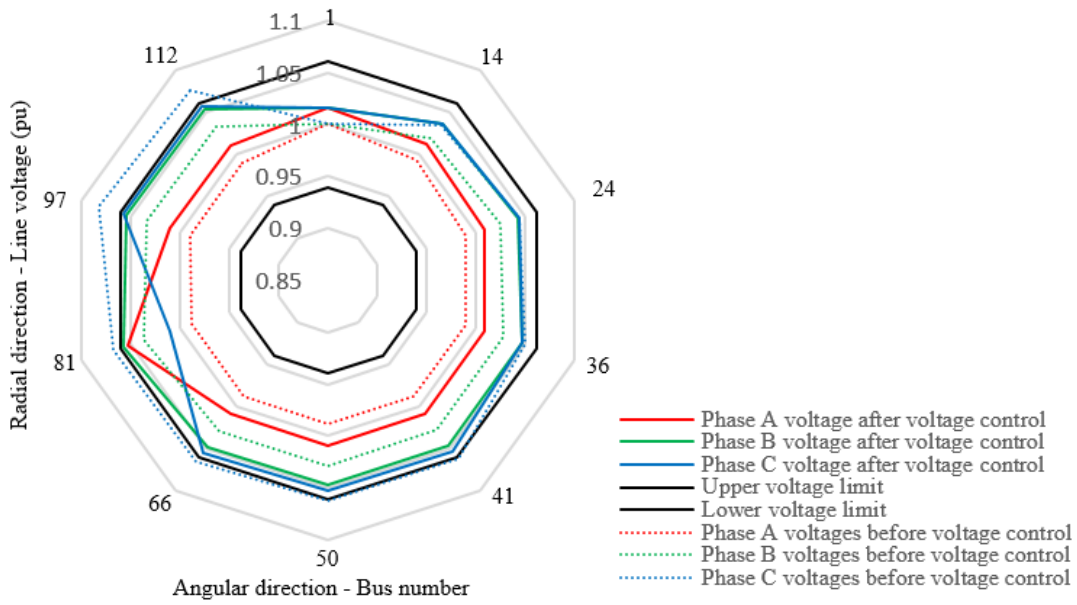

Figure 31 - Voltage profile comparison test case 2

Voltage values of all nodes before voltage control is demonstrated in Figure 32. The voltage rise generated from PV integration can be observed in Figure 31 and Figure 32. The resulting voltage profile after adjusting the taps of OLTC and inverter active/reactive power is included in Figure 33. A comparison between voltage values generated from the optimisation program (simulated using CVX/Mosek) and voltage values generated from load flow (simulated using OpenDSS) at 12.10 p.m is provided in Figure 33 and Figure 34. A small deviation between two voltage profiles verifies the capability of the proposed algorithm to generate exact solutions to the optimum power flow problem. The performance of the algorithm from 12.00 p.m. to 12.50 p.m. is considered next.

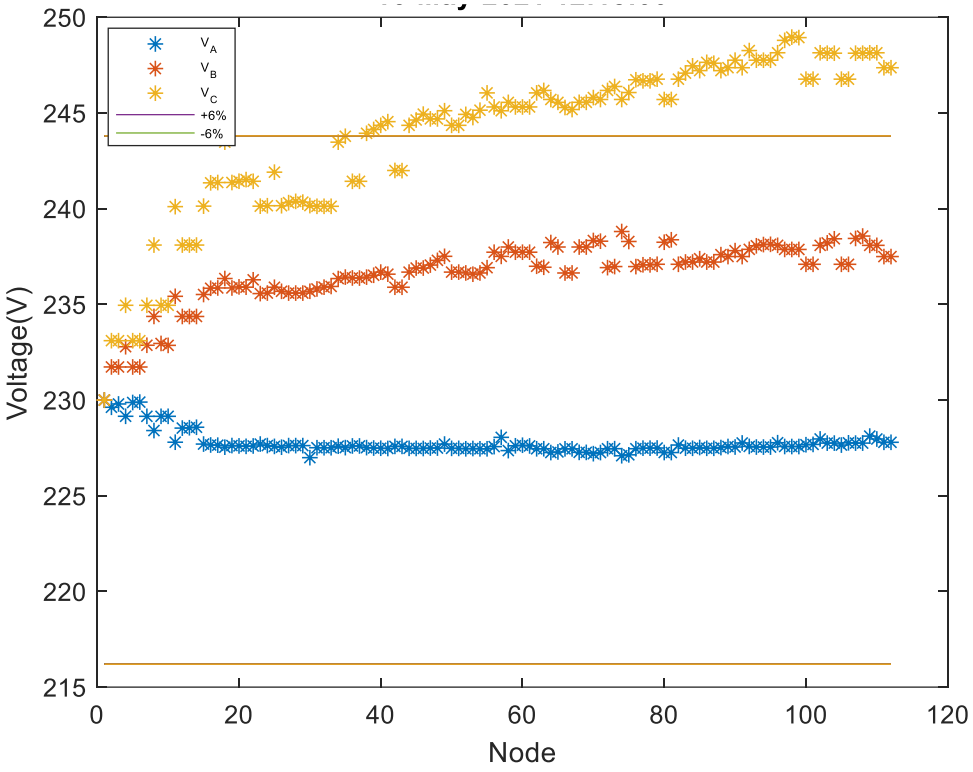

Figure 32 - Voltage profile of case study 2 at 12.10 p.m without using any control scheme

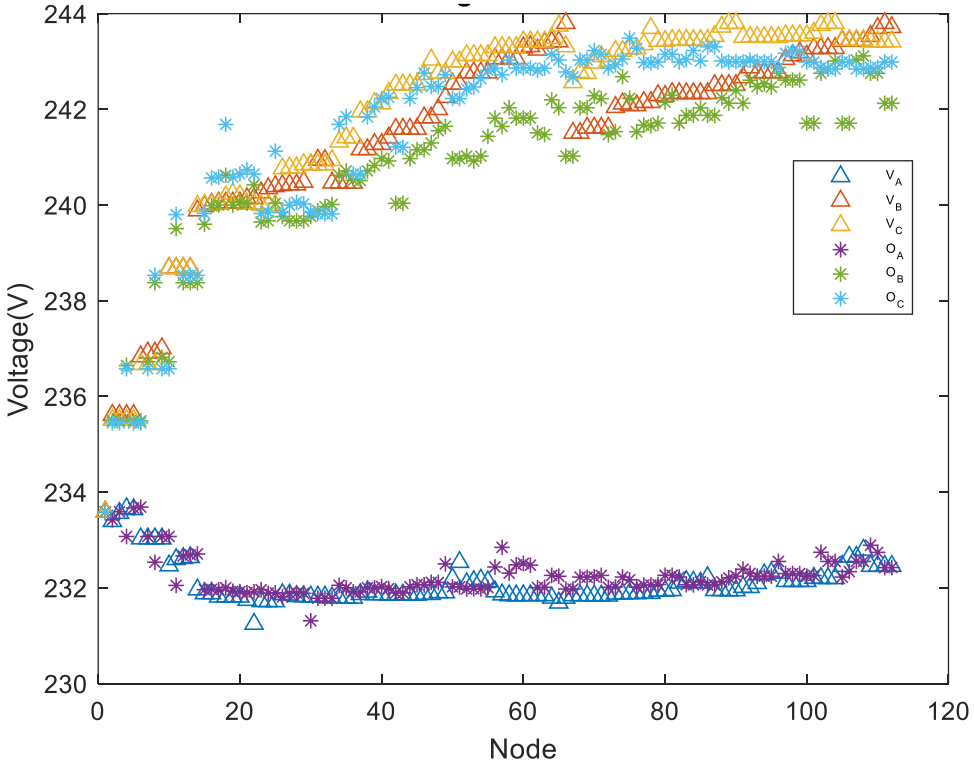

Figure 33 - Voltage profile of case study 2 at 12.10 p.m after using the control algorithm.

Simulation is performed for six-time instances next, to demonstrate the tap operation, line loss and curtailment minimisation. Load profiles at 12.00 a.m, to 12.50 p.m. are selected. Voltage rise above 244 V after 12.10 p.m. in phase C is eliminated after execution of the control algorithm as shown in Figure 35.

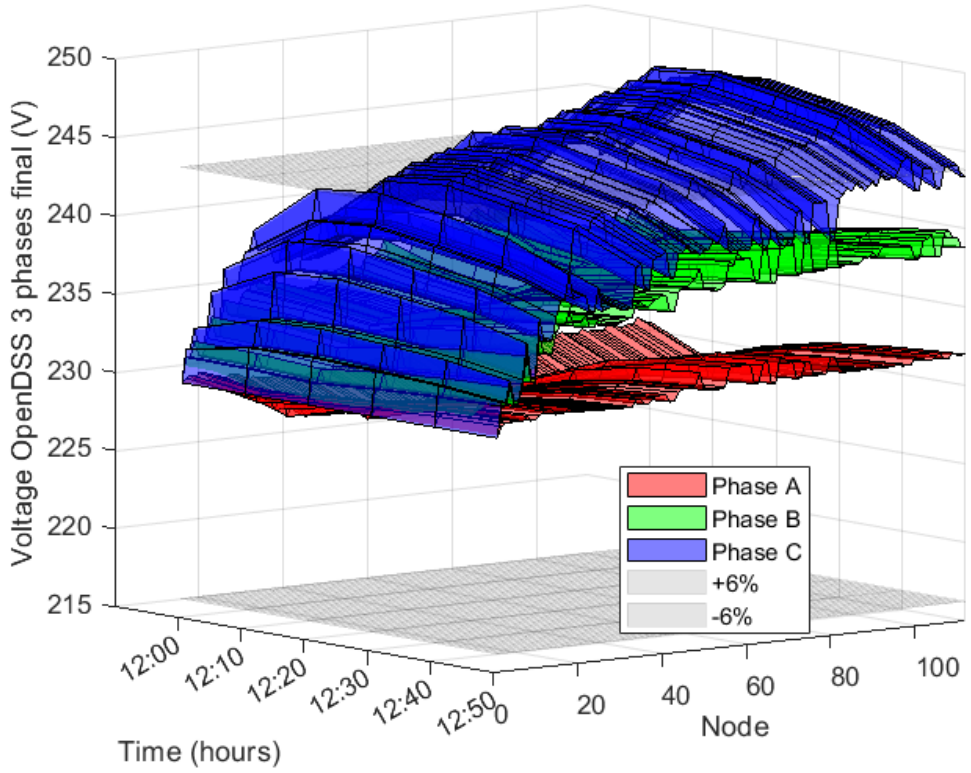

Figure 34 – Voltage profile before voltage control – case study 2

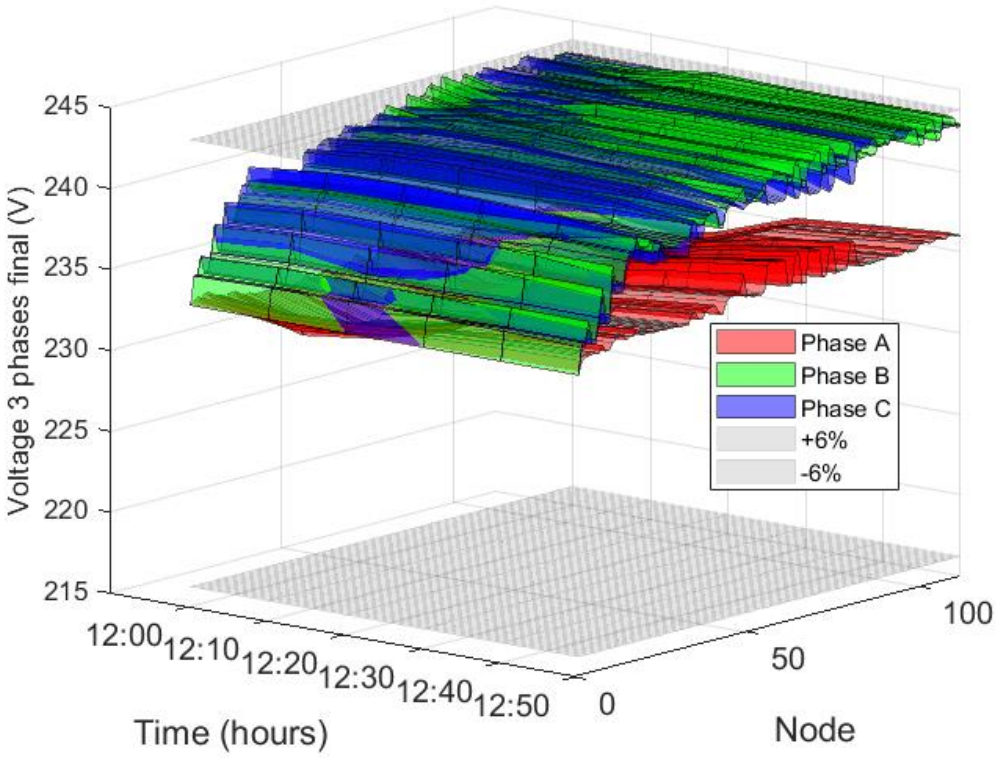

Figure 35 - Voltage profile after voltage control – case study 2

Table 3 - Comparison of outcomes from the algorithm for 3-time instances (test case 2) - 1

Time	Total generation (kW)	Total loads (kW)	Total curtailment (W)	Tap operation
12:00	134.8	36.220	5470	5 to 6
12:10	134.8	31.480	12190	-
12:20	134.8	25.180	13880	-
12:30	134.8	14.680	13710	-
12:40	134.8	9.843	13110	-
12:50	134.8	14.220	9391	-

Table 3, at the start, the default tap position is given as 5 (230.62 V), and in the first 10 minutes, it is adjusted to 6 (233.61 V) from the slow time scale optimisation. By doing this step, line loss is reduced because of higher voltage. Fast time scale

optimisation is executed for remaining 5 time insantces with the tap postion determined by slow time scale optimisation at 12.00 p.m. Tap position is kept at same position for the one hour of slow time scale optimisation.

Table 4 - Comparison of outcomes from the algorithm for 3-time instances (test case 2) -2

Time	Line loss before (W)	Line loss after (W)	Execution time (s)	Exactness (V)
12:00	3143	2652	71.67	0.0423
12:10	4224	2916	75.21	0.2548
12:20	4465	3141	76.62	0.1813
12:30	4763	3375	76.93	0.1766
12:40	4783	3533	77.22	0.1805
12:50	4251	3387	76.79	0.1266

A reduction of line losses is obtained after the execution of the algorithm for all time instances, as shown in Table 4. The average voltage difference is used as a measurement of the exactness of convex optimisation-based methods. This parameter was calculated according to equation (23).

$$\text{Average voltage difference (V)} = \frac{\sum(V_{optimization} - V_{load\ flow})}{number\ of\ nodes} \quad (23)$$

Values of this parameter are provided in Table 4. Demonstrating the accuracy of the proposed algorithm, values of average voltage difference are negligible.

Transformer voltage from 11.00 a.m to 14.50 p.m is provided in Figure 36. In all time instances, fast time scale optimisation is feasible to solve the OPF during one-hour period between slow time scale optimisations. Only one tap operation was performed during this period.

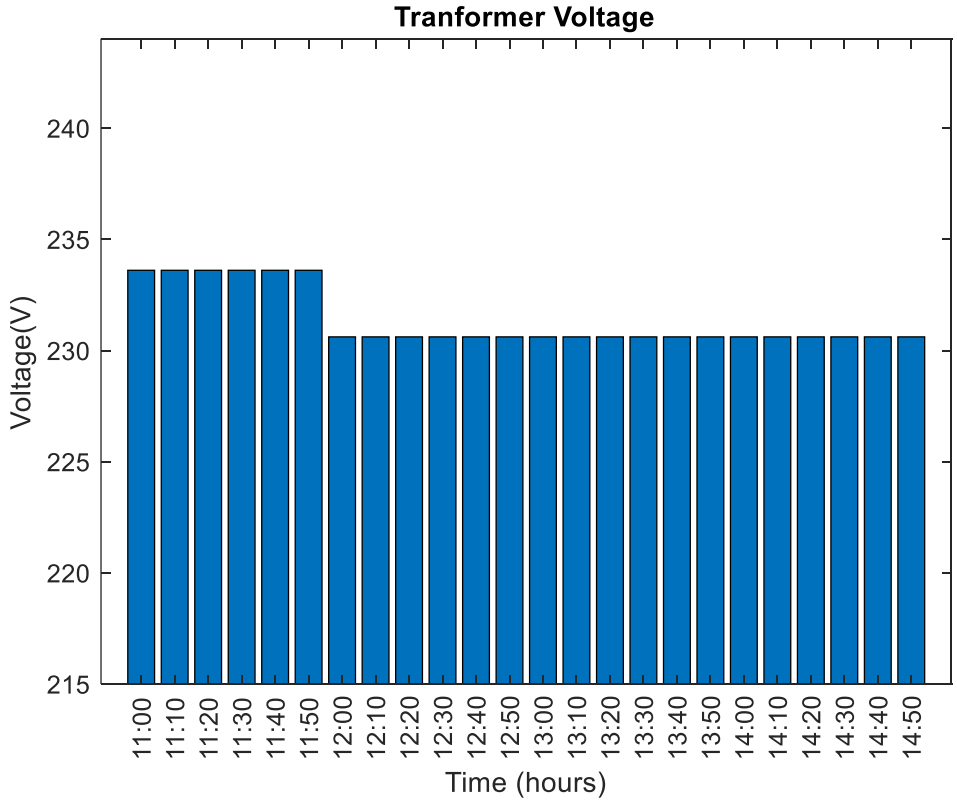

Figure 36 - Transformer voltage (10.00 a.m. - 02.50 p.m.)

4.3 Comparison with other optimisation methods

The following optimisation techniques are implemented and compared with the methodology suggested in this paper. The flow chart shown in Figure 37 was used for genetic algorithm and particle swarm methods described in subsequent sections.

4.3.1 Linear programming-based technique

The methodology suggested in [37] was implemented and used for the comparison. In this method, the nonlinear terms in load flow equations have been replaced with first-order Taylor approximations, and it was assumed that voltage magnitudes of three-phases of the same node are nearly similar. A load flow was performed using OpenDSS to provide operating points for linearization. Only active power curtailment and reactive power compensation are used in [37] for voltage rise mitigation. OLTC is added for the originally proposed algorithm using the same equation used in the method suggested in this thesis. The method was implemented using CVX in Matlab.

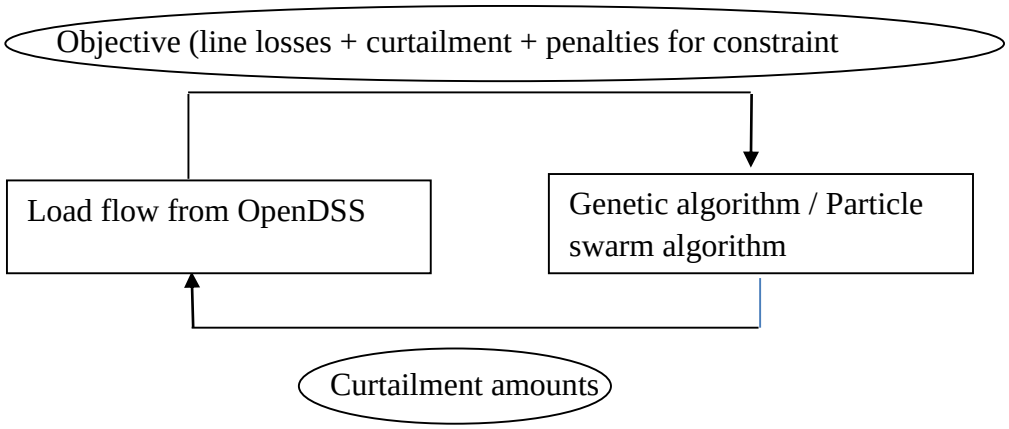

Figure 37 - Flow chart of evolutionary optimisation algorithms

4.3.2 Genetic Algorithm Optimisation

Genetic algorithm-based OPFs were implemented using Matlab functions. Default values of Matlab built-in function were used for reproduction, mutation, cross-over, and migration options. Voltage constraints were added as penalty functions to the objective function. Curtailment is utilized as the only voltage control method due to high execution time. For test case 1, 50 generations were simulated. For test case 2, the genetic algorithm method is not simulated because of the high execution time. The flow chart of the genetic algorithm based OPF problem-solving algorithm is provided in Figure 37.

4.3.3 Particle Swarm Optimisation

Particle swarm optimisation algorithm-based OPFs were implemented using Matlab functions. Default values of the Matlab built-in function were used. For test case 1, 50 iterations were simulated. Active power curtailment is used as the only voltage control method due to high execution time. For test case 2, the genetic algorithm method is not simulated because of the high execution time. The flow chart of the particle swarm-based OPF problem-solving algorithm is provided in Figure 37.

4.3.4 Simulation results comparison – test case 1

A comparison of the simulation results of test case 1 is provided in Table 5. Line losses were obtained from the load flow executed in OpenDSS after including curtailment values, reactive power compensation, and transformer voltages generated from the optimisation program. Only curtailment values were included in genetic algorithm and particle swarm simulations. A comparison of phase B voltage profiles is provided in Figure 38.

As demonstrated in Figure 38, the voltage rise is successfully mitigated using all the methods. The execution times of the evolutionary computing methods (genetic algorithm and particle swarm) are significantly higher than the convex optimisation-based methods (linear program and proposed methods) even though the number of variables is less than half of the variables in convex optimisation-based methods. Therefore, it is clear that the evolutionary computation based methods are not suitable for the real-time application considered in this study. For test case 1, the linear program has superior performance compared to the proposed method in all the analysed components except the average voltage difference. Since the average voltage difference is small both the proposed method and the linear program can be used for test case 1. However suitable optimisation method should be selected considering the performance after applying to a real-world network.

Table 5 - Simulation results comparison (test case 1)

	Proposed method	Linear program	Genetic algorithm (Matlab built-in function)	Particle swarm (Matlab built-in function)
Execution time (s) at 12.00 p.m.	33	4.13	3696.99	4974.93
Tap changes within 12.00 p.m. to 1.00 p.m. with 10-minute intervals	11	6	Not included in the simulation	Not included in the simulation
Line losses (W) at 12.00 p.m.	559.1	660.1	359.9	363.5
Curtailment (W) at 12.00 p.m.	526.1	0	1891.5	1667.8
Average voltage difference (V) at 12.00 p.m	0.15	0.21	0	0

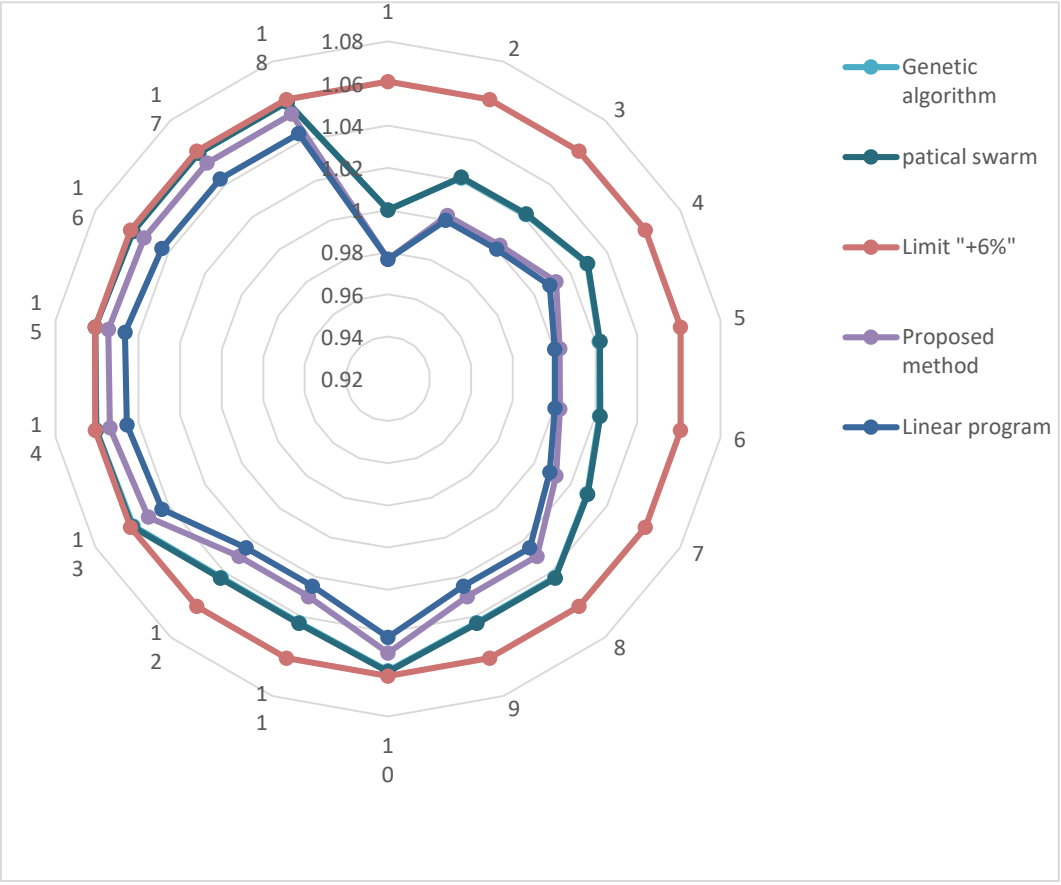

Figure 38 - Test case 1 phase B voltage comparison (pu) at 12.00 p.m

4.3.5 Simulation results comparison – test case 2

A comparison of the simulation results of test case 2 is provided in Table 6. Only the linear program and the proposed method are compared since the execution time of other methods are too high for the application. Line losses were obtained from the load flow executed in OpenDSS after including curtailment values, reactive power compensation and transformer voltages generated from the optimisation program. A comparison of phase C voltage profiles is provided in Figure 39.

As shown in Figure 39 the voltages are within the allowable range in both the linear program and the proposed method. The average voltage difference is significantly high in the linear program based method. The voltage difference at node 112 and close by nodes are nearly 6 V as shown in Figure 41.The V_A, V_B, V_C are voltage values generated from the optimisation program (linear program and proposed method) when

determining minimum cost operation setpoints, O_A, O_B, O_C are voltage values generated from the load flow executed using transformer voltage, curtailment values and reactive power compensation values, generated from the optimisation program. This is occurring due to linearizing approximations used when converting to a linear program. Since voltages in the optimisation program satisfy the voltage constraints, the voltage difference between the optimisation program and load flow can result in a voltage violation in the actual system. For example, the actual voltage of the system can be 250 V in many nodes after applying the set points provided by the linear program method due to the 6 V voltage difference. Therefore, it can be concluded that the linear program is not a suitable method for reliable voltage control in LVDN. As demonstrated in Figure 40, the voltage deviation in the proposed method is sufficient for practical applications.

Table 6 - Simulation results comparison (test case 2)

	Proposed method	Linear program
Execution time (s) at 12.00 p.m.	165	23.17
Tap changes within 12.00 p.m. to 12.10 p.m with 5-minute intervals	2	3
Line losses (W) at 12.00 p.m.	3128	2390.1
Curtailment (W) at 12.00 p.m.	0.14	0
Average voltage difference (V) at 12.00 p.m.	0.024	2.12

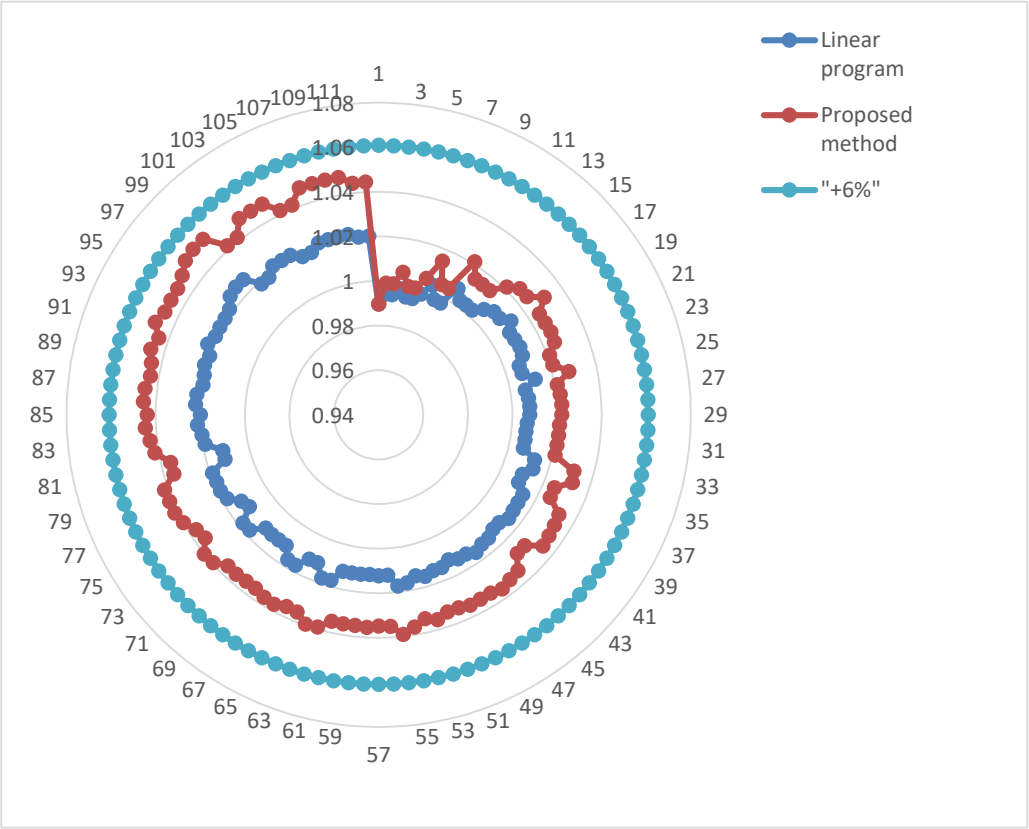

Figure 39 - Test case 2 phase C voltage comparison (pu) at 12.00 p.m

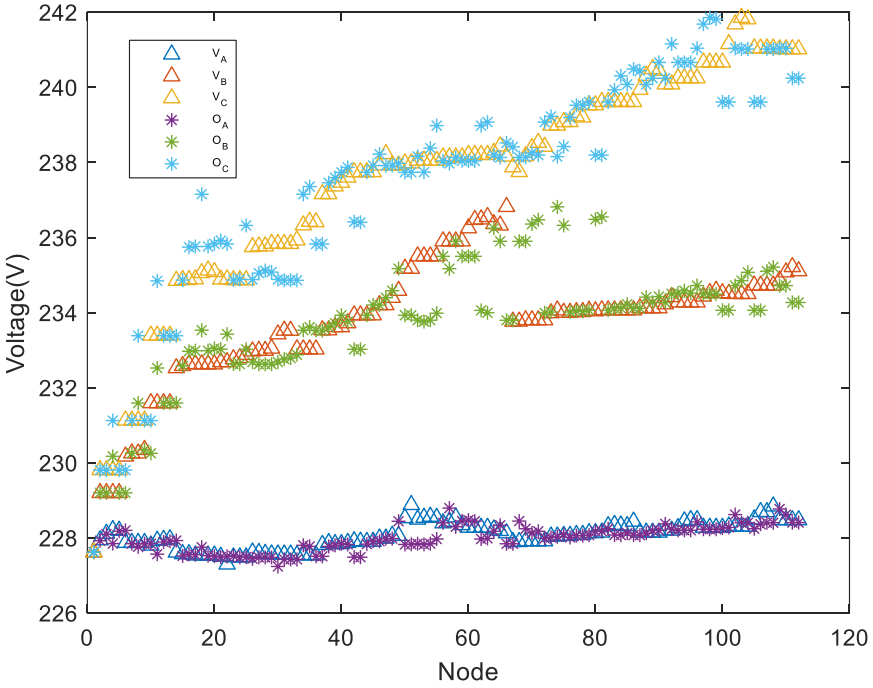

Figure 40 - Voltage profile test case 2 at 12.00 p.m. (Proposed method)

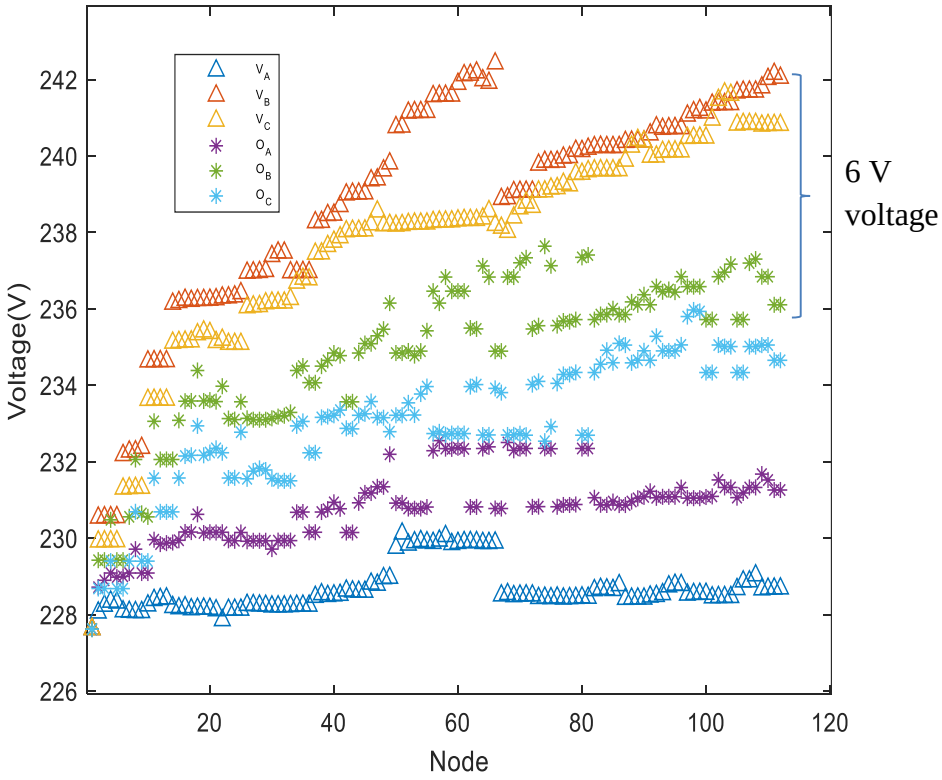

Figure 41 - Voltage profile test case 2 at 12.00 p.m. (Linear program)

5 CONCLUSION

Voltage rise resulting from high solar penetration is a common problem faced by distribution network operators. Voltage rise can be mitigated using voltage control from OLTC transformers, reactive power compensation, and active power curtailment from smart PV inverters. Each of these actions implies a cost and they should be optimised. For example, (a) excessive tap operations of an OLTC will reduce the lifetime of the device, (b) active power curtailment is an energy loss, and (c) reactive power absorption from PV inverters incur more line losses. Therefore, the number of operations of an OLTC, reactive power control of smart PV inverters and active power curtailments should be carried out to optimise the overall cost. Since PV generations and power consumption of loads change in real-time, minimum cost incurring operating setpoints of OLTC and smart inverters need to be calculated in real-time. Therefore, an OPF technique that is fast and accurate for determining the minimum cost incurring set points for OLTC and smart inverters were developed.

Optimum power flow solving algorithms running in two time scales are used to control OLTC and smart inverters. In slow time scale OPF, the optimisation problem was formulated as a radial OPF that minimises the cost of tap operations, line losses, and inverter active power curtailment for unbalanced distribution systems. The problem is a non-convex optimisation problem, and it was converted to a MISOCP problem using relaxations and approximations. Line loss, active power curtailment reduction in PV inverters, and tap operation reduction in OLTC are considered as the objective of MISOCP. Then MISOCP problem was solved for three iterations while tightening the second-order cone relaxations and updating the approximations with load flow data. In fast time scale optimum power flow problem, tap position which was obtained from slow time scale optimisation, was kept as a constant. Fast time scale OPF is a SOCP and the same technique used in slow time scale OPF is used to solve the fast time scale OPF. The proposed algorithm is tested for two test cases. One smaller test case is used to analyse the performance of the algorithm closely. Test case 2 is a real-world LVDN. The performance of the algorithm was evaluated in terms of preventing voltage rise, optimality, execution time and accuracy. Finally, the proposed algorithm is compared with three other OPF problem-solving techniques after implementing them and simulating them for the same test cases.

Simulation results validated the capability of the proposed technique in controlling voltage to mitigate voltage rise while reducing line losses with negligible PV curtailment. The algorithm provided optimum reactive power injection amounts of smart inverters to avoid voltage rise and reduce the cost incurred due to line loss, curtailment and tap change, as demonstrated in the simulation results.

When using convex optimisation-based methods to solve OPF, relaxations and approximations are used to convert the problems to convex optimisation problems. Approximations and relaxations introduce inaccuracies to the solutions. Therefore, testing the exactness is required for convex optimisation-based methods. In this study voltage values obtained from a load flow are used as the voltages of actual LVDN to compare against the voltage values obtained from the proposed method. The deviation between the voltage profiles generated from the optimisation program and load flow is negligible. The average voltage difference is 0.024 V for the real-world test case at 12.00 p.m. Therefore, unexpected voltage deviations after the application of generated set-points of OLTC and inverters is avoided. According to comparison, the inaccuracy of the linear program based method is too high to be used in practical applications.

A faster convex optimisation approach that has a polynomial-time solution algorithm was utilised. The execution time for the real-world test case is around 165 s. The algorithm was developed to obtain exact solutions using increasingly tightening cutting planes in relaxations. The proposed method is much faster than evolutionary computing-based methods as shown in the comparison section. The linear program based method is faster since there is only one iteration of the linear program. But, it is not usable for real-world test case due to the larger difference of calculated voltages from actual voltages. Therefore, from the compared methods, the proposed method is the fastest usable OPF solving technique for real-time optimisation of LVDN with OLTC transformer and smart PV inverters.

5.1 Limitations of the study and proposals for future work

Even though the proposed algorithm is sufficiently fast, communicating measurements can be delayed with the use of low-cost wireless communication. Also, installing communicating devices in every inverter is costly. Voltage measurements can be distorted due to momentarily voltage fluctuations because of cloud passing. In these

situations, the proposed optimisation method can be integrated with a suitable state estimation algorithm to obtain measurements of some inverters.

Line losses and curtailment values are weighted against the cost of tap operation using the cost of energy loss for thirty minutes. It was assumed that the same line loss and curtailment would remain for the next thirty minutes when the optimisation algorithm is executed in every five-minute interval. The weighting of line losses and curtailment components in the objective function can be made further accurate by incorporating load and generation prediction algorithms to determine the weights of curtailment and line loss minimisation components.

Since a polynomial-time algorithm for solving non-convex optimisation problems has not been found yet, there are possibilities to find more optimum, faster and accurate algorithms to solve the OPF problem in LVDNs. In addition to using mathematical techniques to further improve performance, additional computing power can be used to increase the performance of the algorithm. To use the advantage of parallel computing, the proposed algorithm can be implemented in a graphical processing unit.

The proposed method in this study is designed for radial distribution systems. Further improvements can be introduced to use the proposed method in meshed networks. A conic optimisation method is introduced for balanced three-phase systems in [61]. Summation of voltage angle difference is made zero for each loop as additional constrained in [61]. In [62], by selecting breakpoints, a meshed network is converted to a radial configuration. To keep the same operating condition, the branch currents interrupted by the formulation of every breakpoint is restored by current injections at its two end nodes. Similar techniques can be incorporated into the proposed method in this study as future works.

REFERENCES

[1] F. Katiraei and J. R. Agüero, "Solar PV integration challenges," *IEEE Power Energy Mag.*, vol. 9, no. 3, pp. 62–71, 2011, doi: 10.1109/MPE.2011.940579.

[2] C. L. Masters, "Voltage rise the big issue when connecting embedded generation to long 11 kv overhead lines," *Power Eng. J.*, vol. 16, no. 1, pp. 5–12, 2002, doi: 10.1049/pe:20020101.

[3] E. Demirok *et al.*, "Local Reactive Power Control Methods for Overvoltage Prevention of Distributed Solar Inverters in Low-Voltage Grids," *Ieee J. Photovoltaics*, vol. 1, no. 2, pp. 174–182, 2011.

[4] A. R. Malekpour and A. Pahwa, "A Dynamic Operational Scheme for Residential PV Smart Inverters," *IEEE Trans. Smart Grid*, vol. 8, no. 5, pp. 2258–2267, 2017, doi: 10.1109/TSG.2016.2521367.

[5] E. Demirok, D. Sera, P. Rodriguez, and R. Teodorescu, "Enhanced local grid voltage support method for high penetration of distributed generators," *IECON Proc. (Industrial Electron. Conf.*, no. May 2014, pp. 2481–2485, 2011, doi: 10.1109/IECON.2011.6119699.

[6] A. Safayet, P. Fajri, and I. Husain, "Reactive Power Management for Overvoltage Prevention at High PV Penetration in Low Voltage Distribution System," vol. 9994, no. c, 2017, doi: 10.1109/TIA.2017.2741925.

[7] K. De Brabandere, B. Bolsens, J. Van Den Keybus, A. Woyte, J. Driesen, and R. Belmans, "A voltage and frequency droop control method for parallel inverters," *PESC Rec. - IEEE Annu. Power Electron. Spec. Conf.*, vol. 4, no. 2, pp. 2501–2507, 2004, doi: 10.1109/PESC.2004.1355222.

[8] R. Tonkoski and L. A. C. Lopes, "Impact of active power curtailment on overvoltage prevention and energy production of PV inverters connected to low voltage residential feeders," *Renew. Energy*, vol. 36, no. 12, pp. 3566–3574, 2011, doi: 10.1016/j.renene.2011.05.031.

[9] D. E. Mawarni, M. M. V. M. Ali, P. H. Nguyen, W. L. Kling, and M. Jerele, "A case study of using OLTC to mitigate overvoltage in a rural european low voltage network," *Proc. Univ. Power Eng. Conf.*, vol. 2015-Novem, no. 608998, 2015, doi: 10.1109/UPEC.2015.7339875.

[10] S. Yonezawa *et al.*, "Study on a Voltage Estimation of Tap-Changing Transformer in Consideration of SVC Introduction," *Electr. Eng. Japan (English Transl. Denki Gakkai Ronbunshi)*, vol. 199, no. 4, pp. 3–12, 2017, doi: 10.1002/eej.22930.

[11] C. Long and L. F. Ochoa, "Voltage control of PV-rich LV networks: OLTC-fitted transformer and capacitor banks," *IEEE Trans. Power Syst.*, vol. 31, no.

5, pp. 4016–4025, 2016, doi: 10.1109/TPWRS.2015.2494627.

[12] A. Navarro-espinosa and L. F. Ochoa, “Increasing the PV Hosting Capacity of LV Networks : OLTC-Fitted Transformers vs . Reinforcements,” pp. 2011–2014, 2015.

[13] X. Liu, A. Aichhorn, L. Liu, and H. Li, “Coordinated control of distributed energy storage system with tap changer transformers for voltage rise mitigation under high photovoltaic penetration,” *IEEE Trans. Smart Grid*, vol. 3, no. 2, pp. 897–906, 2012, doi: 10.1109/TSG.2011.2177501.

[14] C. Y. Lau, C. K. Gan, Z. Salam, and M. F. Sulaima, “Impact of Solar Photovoltaic System on Transformer Tap Changer in Low Voltage Distribution Networks,” *Energy Procedia*, vol. 103, no. December, pp. 58–63, 2016, doi: 10.1016/j.egypro.2016.11.249.

[15] G. Fei, Z. Shuqi, Y. Kuo, L. Jinzhong, Z. Shirui, and D. Benping, “Study on arcless switching experiments of hybrid on-load tap changer in transformers,” *POWERCON 2014 - 2014 Int. Conf. Power Syst. Technol. Towar. Green, Effic. Smart Power Syst. Proc.*, no. Powercon, pp. 1287–1292, 2014, doi: 10.1109/POWERCON.2014.6993583.

[16] S. Boyd and L. Vandenberghe, *Convex Optimisation*, 07 ed. Cambridge University Press., 2009.

[17] Numerical Algorithms Group Ltd, “Second-order Cone Programming (SOCP),” 2021. https://www.nag.com/content/second-order-cone-programming-socp-0.

[18] K. Schittkowski and C. Zillober, “Sequential Convex Programming Methods,” pp. 123–141, 1995, doi: 10.1007/978-3-642-88272-2_8.

[19] J. Carpentier, “Optimal power flows,” vol. 1, no. 1, pp. 3–15, 1979.

[20] S. Frank, I. Steponavice, and S. Rebennack, “Optimal power flow: A bibliographic survey I Formulations and deterministic methods,” *Energy Syst.*, vol. 3, no. 3, pp. 221–258, 2012, doi: 10.1007/s12667-012-0056-y.

[21] C. Coffrin and P. Van Hentenryck, “A Linear-Programming Approximation of AC Power Flows,” *INFORMS J. Comput.*, pp. 1–13, 2014, doi: 10.1287/ijoc.2014.0594.

[22] R. Bacher and H. P. Van Meeteren, “REAL-TIME OPTIMAL POWER FLOW IN AUTOMATIC GENERATION CONTROL,” *IEEE Trans. Power Syst.*, vol. 3, no. 4, p. 6, 1988.

[23] E. Mohagheghi, M. Alramlawi, A. Gabash, and P. Li, “A survey of real-time optimal power flow,” *Energies*, vol. 11, no. 11, 2018, doi: 10.3390/en11113142.

[24] P. Siano, C. Cecati, F. Ieee, H. Yu, and S. Member, “Real Time Operation of

Smart Grids via FCN Networks and Optimal Power Flow," no. c, 2011.

[25] K. Mahmoud, M. M. Hussein, M. Abdel-Nasser, and M. Lehtonen, "Optimal Voltage Control in Distribution Systems with Intermittent PV Using Multiobjective Grey-Wolf-Lévy Optimizer," *IEEE Syst. J.*, vol. 14, no. 1, pp. 760–770, 2020, doi: 10.1109/JSYST.2019.2931829.

[26] T. Senjyu, Y. Miyazato, A. Yona, N. Urasaki, and T. Funabashi, "Optimal distribution voltage control and coordination with distributed generation," *IEEE Trans. Power Deliv.*, vol. 23, no. 2, pp. 1236–1242, 2008, doi: 10.1109/TPWRD.2007.908816.

[27] S. Y. Abdelouadoud, R. Girard, F. P. Neirac, and T. Guiot, "Optimal power flow of a distribution system based on increasingly tight cutting planes added to a second order cone relaxation," *Int. J. Electr. Power Energy Syst.*, vol. 69, pp. 9–17, 2015, doi: 10.1016/j.ijepes.2014.12.084.

[28] Q. Li and V. Vittal, "Convex Hull of the Quadratic Branch AC Power Flow Equations and Its Application in Radial Distribution Networks," *IEEE Trans. Power Syst.*, vol. 2016, no. 1, pp. 1–9, 2017, doi: 10.1109/TPWRS.2017.2712697.

[29] X. Bai, H. Wei, K. Fujisawa, and Y. Wang, "Semidefinite programming for optimal power flow problems," *Int. J. Electr. Power Energy Syst.*, vol. 30, no. 6–7, pp. 383–392, 2008, doi: 10.1016/j.ijepes.2007.12.003.

[30] E. Dall'Anese, G. B. Giannakis, and B. F. Wollenberg, "Optimisation of unbalanced power distribution networks via semidefinite relaxation," *2012 North Am. Power Symp. NAPS 2012*, 2012, doi: 10.1109/NAPS.2012.6336350.

[31] L. Gan and S. H. Low, "Convex relaxations and linear approximation for optimal power flow in multiphase radial networks," *Proc. - 2014 Power Syst. Comput. Conf. PSCC 2014*, 2014, doi: 10.1109/PSCC.2014.7038399.

[32] M. Farivar, R. Neal, C. Clarke, and S. Low, "Optimal inverter VAR control in distribution systems with high PV penetration," *IEEE Power Energy Soc. Gen. Meet.*, pp. 1–7, 2012, doi: 10.1109/PESGM.2012.6345736.

[33] Z. Yuan and M. R. Hesamzadeh, "Second-order cone AC optimal power flow: convex relaxations and feasible solutions," *J. Mod. Power Syst. Clean Energy*, vol. 7, no. 2, pp. 268–280, 2019, doi: 10.1007/s40565-018-0456-7.

[34] S. H. Low, "Convex relaxation of optimal power flow - Part i: Formulations and equivalence," *IEEE Trans. Control Netw. Syst.*, vol. 1, no. 1, pp. 15–27, 2014, doi: 10.1109/TCNS.2014.2309732.

[35] H. Ji *et al.*, "An enhanced SOCP-based method for feeder load balancing using the multi-terminal soft open point in active distribution networks," *Appl. Energy*, vol. 208, no. August, pp. 986–995, 2017, doi:

10.1016/j.apenergy.2017.09.051.

[36] N. Nazir, P. Racherla, and M. Almassalkhi, “Optimal Multi-Period Dispatch of Distributed Energy Resources in Unbalanced Distribution Feeders,” *IEEE Trans. Power Syst.*, vol. 35, no. 4, pp. 2683–2692, 2020, doi: 10.1109/TPWRS.2019.2963249.

[37] B. A. Robbins and A. D. Domínguez-García, “Optimal Reactive Power Dispatch for Voltage Regulation in Unbalanced Distribution Systems,” *IEEE Trans. Power Syst.*, vol. 31, no. 4, pp. 2903–2913, 2016, doi: 10.1109/TPWRS.2015.2451519.

[38] X. Su, M. A. S. Masoum, and P. J. Wolfs, “Optimal PV Inverter Reactive Power Control and Real Power Curtailment to Improve the Performance of Low Voltage Distribution System,” *IEEE Trans. Sustain. Energy*, vol. 5, no. 3, pp. 967–977, 2014.

[39] C. Li, V. R. Disfani, Z. K. Pecenak, S. Mohajeryami, and J. Kleissl, “Optimal OLTC voltage control scheme to enable high solar penetrations,” *Electr. Power Syst. Res.*, vol. 160, pp. 318–326, 2018, doi: 10.1016/j.epsr.2018.02.016.

[40] B. A. Robbins, H. Zhu, and A. D. Dominguez-Garcia, “Optimal tap setting of voltage regulation transformers in unbalanced distribution systems,” *IEEE Trans. Power Syst.*, vol. 31, no. 1, pp. 256–267, 2016, doi: 10.1109/TPWRS.2015.2392693.

[41] W. Sheng, K. Y. Liu, S. Cheng, X. Meng, and W. Dai, “A trust region SQP method for coordinated voltage control in smart distribution grid,” *IEEE Trans. Smart Grid*, vol. 7, no. 1, pp. 381–391, 2016, doi: 10.1109/TSG.2014.2376197.

[42] C. Lin, H. Wei, W. Hou, and J. Tan, “Linear inequalities convex transformation for optimal reactive power flow model based on MISOCP relaxations,” pp. 1589–1594, 2018, doi: 10.1049/iet-gtd.2017.1714.

[43] Z. Tian, W. Wu, B. Zhang, and A. Bose, “Mixed-integer second-order cone programing model for VAR optimisation and network reconfiguration in active distribution networks,” *IET Gener. Transm. Distrib.*, vol. 10, no. 8, pp. 1938–1946, 2016, doi: 10.1049/iet-gtd.2015.1228.

[44] S. R. Shukla, S. Member, S. Paudyal, and M. R. Almassalkhi, “Efficient Distribution System Optimal Power Flow with Discrete Control of Load Tap Changers,” vol. 8950, no. c, pp. 1–10, 2019, doi: 10.1109/TPWRS.2019.2894674.

[45] R. Louca, P. Seiler, and E. Bitar, “A rank minimisation algorithm to enhance semidefinite relaxations of Optimal Power Flow,” *2013 51st Annu. Allert. Conf. Commun. Control. Comput. Allert. 2013*, pp. 1010–1020, 2013, doi: 10.1109/Allerton.2013.6736636.

[46] B. C. Lesieutre, D. K. Molzahn, A. R. Borden, and C. L. DeMarco, "Examining the limits of the application of semidefinite programming to power flow problems," *2011 49th Annu. Allert. Conf. Commun. Control. Comput. Allert. 2011*, pp. 1492–1499, 2011, doi: 10.1109/Allerton.2011.6120344.

[47] R. M. and J. L. Somayeh Sojoudi*, "Low-Rank Solution of Convex Relaxation for Optimal Power Flow Problem," in *IEEE SmartGridComm 2013 Symposium - Support for Storage, Renewable Resources and Micro-grids*, 2013, pp. 636–641.

[48] H. Hijazi, C. Coffrin, and P. Van Hentenryck, "Convex quadratic relaxations for mixed-integer nonlinear programs in power systems," *Math. Program. Comput.*, vol. 9, no. 3, pp. 321–367, 2017, doi: 10.1007/s12532-016-0112-z.

[49] L. Gan, N. Li, U. Topcu, and S. H. Low, "Exact Convex Relaxation of Optimal Power Flow in Radial Networks," *IEEE Trans. Automat. Contr.*, vol. 60, no. 1, pp. 72–87, 2015, doi: 10.1109/TAC.2014.2332712.

[50] S. H. Low, "Convex relaxation of optimal power flow-part II: Exactness," *IEEE Trans. Control Netw. Syst.*, vol. 1, no. 2, pp. 177–189, 2014, doi: 10.1109/TCNS.2014.2323634.

[51] J.-P. Watson, A. Castillo, P. Lipka, S. Oren, and R. O'Neill, "A Current-Voltage Successive Linear Programming Approach to Solving the ACOPF.," *IEEE Trans. Power Syst.*, pp. 1–8, 2014.

[52] Z. Yang, H. Zhong, Q. Xia, A. Bose, and C. Kang, "Optimal power flow based on successive linear approximation of power flow equations," *IET Gener. Transm. Distrib.*, vol. 10, no. 14, pp. 3654–3662, 2016, doi: 10.1049/iet-gtd.2016.0547.

[53] A. Gopalakrishnan, A. U. Raghunathan, D. Nikovski, and L. T. Biegler, "Global optimisation of Optimal Power Flow using a branch & bound algorithm," *2012 50th Annu. Allert. Conf. Commun. Control. Comput. Allert. 2012*, pp. 609–616, 2012, doi: 10.1109/Allerton.2012.6483274.

[54] S. Boyd and J. Mattingley, "Branch and Bound Methods," pp. 1–18, 2018.

[55] Q. Nguyen, S. Member, H. V Padullaparti, S. Member, and K. Lao, "Exact Optimal Power Dispatch in Unbalanced Distribution Systems with High PV Penetration," *IEEE Trans. Power Syst.*, vol. 8950, no. c, pp. 1–10, 2018, doi: 10.1109/TPWRS.2018.2869195.

[56] W. H. Kersting, *Distribution System Modelling and Analysis*. Florida: CRC Press, 2002.

[57] S. L. Public Utilities Commission, "DISTRIBUTION CODE OF SRI LANKA," 2012. [Online]. Available: https://www.ceb.lk/front_img/img_reports/1532500020Distribution_Code.pdf.

[58] and Y. Y. M. Grant, S. Boyd, “CVX: Matlab Software for Disciplined Convex Programming.” http://www.stanford.edu/~boyd/cvx.

[59] J. Hu, M. Marinelli, M. Coppo, A. Zecchino, and H. W. Bindner, “Coordinated voltage control of a decoupled three-phase on-load tap changer transformer and photovoltaic inverters for managing unbalanced networks,” *Electr. Power Syst. Res.*, vol. 131, pp. 264–274, 2016, doi: 10.1016/j.epsr.2015.10.025.

[60] I. P. and energy Soceity, “European Low Voltage Test Feeder,” *IEEE Power and energy Soceity*, 2015. https://site.ieee.org/pes-testfeeders/resources/ (accessed Feb. 14, 2020).

[61] R. A. Jabr, “A conic quadratic format for the load flow equations of meshed networks,” *IEEE Trans. Power Syst.*, vol. 22, no. 4, pp. 2285–2286, 2007, doi: 10.1109/TPWRS.2007.907590.

[62] D. Shirmohammadi, H. W. Hong, A. Semlyen, and G. X. Luo, “A compensation-based power flow method for weakly meshed distribution and transmission networks,” *IEEE Trans. Power Syst.*, vol. 3, no. 2, pp. 753–762, 1988, doi: 10.1109/59.192932.

APPENDIX A

Table 7 - Details of cable of test case 1

Name	Bus1	Bus2	Length	Units	Cable type
LINE1	1	2	220	m	4c_70
LINE2	2	3	6	m	2c_16
LINE3	2	4	120	m	4c_70
LINE4	3	5	3	m	2c_16
LINE5	3	6	4	m	2c_16
LINE6	4	7	10	m	2c_16
LINE7	4	8	220	m	4c_70
LINE8	8	9	9	m	2c_16
LINE9	8	10	260	m	4c_70
LINE10	9	11	4	m	2c_16
LINE11	9	12	4	m	2c_16
LINE12	10	13	17	m	2c_16
LINE13	10	14	120	m	4c_70
LINE14	14	15	15	m	2c_16
LINE15	14	16	120	m	4c_70
LINE16	16	17	15	m	2c_16
LINE17	16	18	21	m	2c_16

Impedances of cable types used in case studies are provided in Table 8. Types of each cable used in each section is provided in Table 7 – cable type column.

Table 8 – Impedance values of cables used in test cases.

Cable type	phases	Impedance (Ω/ km)					
		R1	X1	R0	X0	C1	C0
'2c_.007'	3	3.97	0.099	3.97	0.099	0	0
'2c_.0225'	3	1.257	0.085	1.257	0.085	0	0
'2c_16'	3	1.15	0.088	1.2	0.088	0	0
'35_SAC_XSC'	3	0.868	0.092	0.76	0.092	0	0
'4c_.06'	3	0.469	0.075	1.581	0.091	0	0
'4c_.1'	3	0.274	0.073	0.959	0.079	0	0
'4c_.35'	3	0.089	0.0675	0.319	0.076	0	0
'4c_185'	3	0.166	0.068	0.58	0.078	0	0
'4c_70'	3	0.446	0.071	1.505	0.083	0	0
'4c_95_SAC_XC'	3	0.322	0.074	0.804	0.093	0	0

APPENDIX B

The equations (A1) and (A2) were obtained by expanding equations (2) and (3). Variables in non-convex terms ($U_{A}^{R}{}_{n}, I_{A}^{R}{}_{mn}, U_{A}^{Im}{}_{n}, I_{A}^{Im}{}_{mn}$) were replaced from respective values obtained from the load flow. Then, $W_{A_m} = |\boldsymbol{U_{A_m}}|^2$ and $L_{A_{mn}} = |\boldsymbol{I_{A_{mn}}}|^2$ substitutions were made to make the equations linear.

$$p_{A_{mn}} = \sum_{k:(j,k)\in E} p_{A_{nk}} + \mathrm{P}_{\mathrm{A_n}}^{\mathrm{C}} - \mathrm{P}_{\mathrm{A_n}}^{\mathrm{G}} + \mathrm{R}_{\mathrm{s_{mn}}} L_{A_{mn}} + \mathrm{R}_{\mathrm{m_{mn}}}\left(I_{A}^{R}{}_{mn}\, I_{B}^{R}{}_{mn} + I_{A}^{Im}{}_{mn}\, I_{B}^{Im}{}_{mn}\right) - \mathrm{X}_{\mathrm{m_{mn}}}\left(I_{A}^{R}{}_{mn}\, I_{B}^{Im}{}_{mn} - I_{A}^{Im}{}_{m}\, I_{B}^{R}{}_{m}\right) + \mathrm{R}_{\mathrm{m_{mn}}}\left(I_{A}^{R}{}_{mn}\, I_{C}^{R}{}_{mn} + I_{A}^{Im}{}_{mn}\, I_{C}^{Im}{}_{mn}\right) - \mathrm{X}_{\mathrm{m_{mn}}}\left(I_{A}^{R}{}_{mn}\, I_{C}^{Im}{}_{mn} - I_{A}^{Im}{}_{m}\, I_{C}^{R}{}_{m}\right) \quad \text{(A1)}$$

$$q_{A_{mn}} = \sum_{k:(j,k)\in E} q_{A_{nk}} + \mathrm{Q}_{\mathrm{A_n}}^{\mathrm{C}} + Q_{A_n}^{G} + \mathrm{X}_{\mathrm{s_{mn}}} L_{A_{mn}} + \mathrm{X}_{\mathrm{m_{mn}}}\left(I_{A}^{R}{}_{mn}\, I_{B}^{R}{}_{mn} + I_{A}^{Im}{}_{mn}\, I_{B}^{Im}{}_{mn}\right) + \mathrm{R}_{\mathrm{m_{mn}}}\left(I_{A}^{R}{}_{mn}\, I_{B}^{Im}{}_{mn} - I_{A}^{Im}{}_{m}\, I_{B}^{R}{}_{m}\right) + \mathrm{X}_{\mathrm{m_{mn}}}\left(I_{A}^{R}{}_{mn}\, I_{C}^{R}{}_{mn} + I_{A}^{Im}{}_{mn}\, I_{C}^{Im}{}_{mn}\right) + \mathrm{R}_{\mathrm{m_{mn}}}\left(I_{A}^{R}{}_{mn}\, I_{C}^{Im}{}_{mn} - I_{A}^{Im}{}_{m}\, I_{C}^{R}{}_{m}\right) \quad \text{(A2)}$$

Derivation of equation A4:

$$\mathbf{U_{A_m}} = \left(\mathbf{U_{A_n}} - \mathbf{I_{A_{mn}}Z_S} - \mathbf{I_{B_{mn}}Z_m} - \mathbf{I_{C_{mn}}Z_m}\right) \quad (8)$$

After separating real and, imaginary parts equation (8) was expressed as follows.

$$\begin{aligned}\mathbf{U_{A_m}} = {} & U_{A}^{R}{}_{n} + U_{A}^{Im}{}_{n}j - \left(I_{A}^{R}{}_{mn} + jI_{A}^{Im}{}_{mn}\right)\left(R_{S_{mn}} + jX_{S_{mn}}\right) \\ & - \left(I_{B}^{R}{}_{mn} + jI_{B}^{Im}{}_{mn}\right)\left(R_{m_{mn}} + jX_{m_{mn}}\right) \\ & - \left(I_{C}^{R}{}_{mn} + jI_{C}^{Im}{}_{mn}\right)\left(R_{m_{mn}} + jX_{m_{mn}}\right)\end{aligned}$$

After multiplications between current and resistance terms following equation was obtained.

$$\begin{aligned}U_{A}^{R}{}_{m} + U_{A}^{Im}{}_{m}j = {} & U_{A}^{R}{}_{n} + jU_{A}^{Im}{}_{n} \\ & - \left\{R_{S_{mn}}I_{A}^{R}{}_{mn} + jX_{S_{mn}}I_{A}^{R}{}_{mn} + jR_{S_{mn}}I_{A}^{Im}{}_{mn} - X_{S_{mn}}I_{A}^{Im}{}_{mn}\right\} \\ & - \left\{R_{m_{mn}}I_{B}^{R}{}_{mn} + jX_{m_{mn}}I_{B}^{R}{}_{mn} + jR_{m_{mn}}I_{B}^{Im}{}_{mn} - X_{m_{mn}}I_{B}^{Im}{}_{mn}\right\} \\ & - \left\{R_{m_{mn}}I_{C}^{R}{}_{mn} + jX_{m_{mn}}I_{C}^{R}{}_{mn} + jR_{m_{mn}}I_{C}^{Im}{}_{mn} - X_{m_{mn}}I_{C}^{Im}{}_{mn}\right\}\end{aligned}$$

The squared magnitude of the complex number is obtained after the summation of squares of real and imaginary parts.

$$\begin{aligned}\left|\boldsymbol{U_{A_m}}\right|^2 = {} & \left(U_{A}^{R}{}_{n} - R_{S_{mn}}I_{A}^{R}{}_{mn} + X_{S_{mn}}I_{A}^{Im}{}_{mn} - R_{m_{mn}}I_{B}^{R}{}_{mn} + X_{m_{mn}}I_{B}^{Im}{}_{mn} - \right. \\ & \left. R_{m_{mn}}I_{C}^{R}{}_{mn} + X_{m_{mn}}I_{C}^{Im}{}_{mn}\right)^2 + \left(U_{A}^{Im}{}_{n} - X_{S_{mn}}I_{A}^{R}{}_{mn} - R_{S_{mn}}I_{A}^{Im}{}_{mn} - X_{m_{mn}}I_{B}^{R}{}_{mn} - \right. \\ & \left. R_{m_{mn}}I_{B}^{Im}{}_{mn} - X_{m_{mn}}I_{C}^{R}{}_{mn} - R_{m_{mn}}I_{C}^{Im}{}_{mn}\right)^2\end{aligned} \quad (A3)$$

After expanding above A3, simplification, and substituting from equation (7), equation A4 was obtained.

$$\begin{aligned}W_{A_m} = {} & W_{A_n} + \mathrm{R_{S_{mn}}}^2 L_{A_{mn}} + \mathrm{X_{S_{mn}}}^2 L_{A_{mn}} + \mathrm{R_{m_{mn}}}^2 L_{B_{mn}} + \mathrm{X_{m_{mn}}}^2 L_{B_{mn}} + \\ & \mathrm{R_{m_{mn}}}^2 L_{C_{mn}} + \mathrm{X_{m_{mn}}}^2 L_{C_{mn}} - 2\,p_{mn_A} - 2\,q_{mn_A} - 2V_{A}^{R}{}_{n}\mathrm{R_{m_{mn}}}I_{B}^{R}{}_{mn} + \\ & 2V_{A}^{R}{}_{n}\mathrm{X_{m_{mn}}}I_{B}^{Im}{}_{mn} - 2V_{A}^{R}{}_{n}\mathrm{R_{m_{mn}}}I_{C}^{R}{}_{mn} + 2V_{A}^{R}{}_{n}\mathrm{X_{m_{mn}}}I_{C}^{Im}{}_{mn} - 2V_{A}^{Im}{}_{n}\mathrm{X_{m_{mn}}}I_{B}^{R}{}_{mn} - \\ & 2V_{A}^{Im}{}_{n}\mathrm{R_{m_{mn}}}I_{B}^{Im}{}_{mn} - 2V_{A}^{Im}{}_{n}\mathrm{X_{m_{mn}}}I_{C}^{R}{}_{mn} - 2V_{A}^{Im}{}_{n}\mathrm{R_{m_{mn}}}I_{C}^{Im}{}_{mn} +\end{aligned}$$

$$2R_{S_{mn}} I_{A}^{R}{}_{mn} R_{m_{mn}} I_{B}^{R}{}_{mn} - 2R_{S_{mn}} I_{A}^{R}{}_{mn} X_{m_{mn}} I_{B}^{Im}{}_{mn} + 2R_{S_{mn}} I_{A}^{R}{}_{mn} R_{m_{mn}} I_{C}^{R}{}_{mn} -$$
$$2R_{S_{mn}} I_{A}^{R}{}_{mn} X_{m_{mn}} I_{C}^{Im}{}_{mn} - 2X_{S_{mn}} I_{A}^{Im}{}_{mn} R_{m_{mn}} I_{B}^{R}{}_{mn} + 2X_{S_{mn}} I_{A}^{Im}{}_{mn} X_{m_{mn}} I_{B}^{Im}{}_{mn} -$$
$$2X_{S_{mn}} I_{A}^{Im}{}_{mn} R_{m_{mn}} I_{C}^{R}{}_{mn} - 2X_{S_{mn}} I_{A}^{Im}{}_{mn} X_{m_{mn}} I_{C}^{Im}{}_{mn} + 2R_{m_{mn}} I_{B}^{R}{}_{mn} R_{m_{mn}} I_{C}^{R}{}_{mn} -$$
$$2R_{m_{mn}} I_{B}^{R}{}_{mn} X_{m_{mn}} I_{C}^{Im}{}_{mn} + 2X_{m_{mn}} I_{B}^{Im}{}_{mn} X_{m_{mn}} I_{C}^{Im}{}_{mn} + 2X_{S_{mn}} I_{A}^{R}{}_{mn} X_{m_{mn}} I_{B}^{R}{}_{mn} +$$
$$2X_{S_{mn}} I_{A}^{R}{}_{mn} R_{m_{mn}} I_{B}^{Im}{}_{mn} + 2X_{S_{mn}} I_{A}^{R}{}_{mn} X_{m_{mn}} I_{C}^{R}{}_{mn} + 2X_{S_{mn}} I_{A}^{R}{}_{mn} R_{m_{mn}} I_{C}^{Im}{}_{mn} +$$
$$2R_{S_{mn}} I_{A}^{Im}{}_{mn} X_{m_{mn}} I_{B}^{R}{}_{mn} + 2R_{S_{mn}} I_{A}^{Im}{}_{mn} R_{m_{mn}} I_{B}^{Im}{}_{mn} + 2I_{A}^{Im}{}_{mn} X_{m_{mn}} I_{C}^{R}{}_{mn} +$$
$$2R_{S_{mn}} I_{A}^{Im}{}_{mn} R_{m_{mn}} I_{C}^{Im}{}_{mn} + 2X_{m_{mn}} I_{B}^{R}{}_{mn} X_{m_{mn}} I_{C}^{R}{}_{mn} + 2X_{m_{mn}} I_{B}^{R}{}_{mn} R_{m_{mn}} I_{C}^{Im}{}_{mn} +$$
$$2R_{m_{mn}} I_{B}^{Im}{}_{mn} R_{m_{mn}} I_{C}^{Im}{}_{mn} \qquad \text{(A4)}$$